

Contents lists available at ScienceDirect

Journal of Colloid and Interface Science

journal homepage: www.elsevier.com/locate/jcis



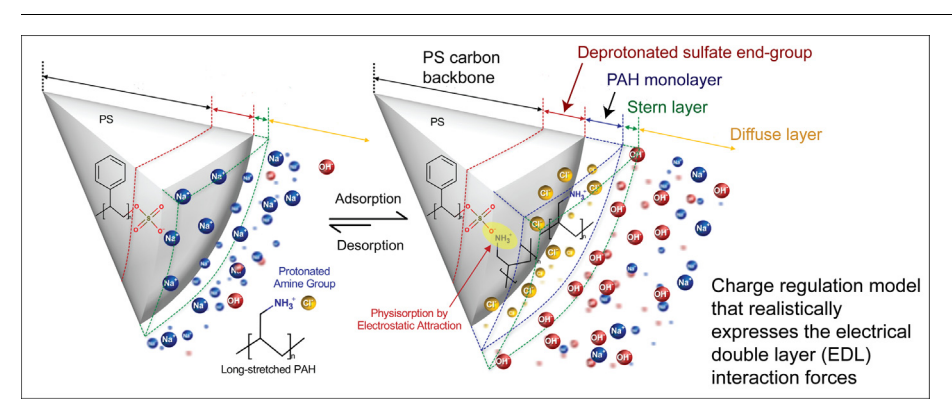
Nonlinear charge regulation for the deposition of silica nanoparticles on polystyrene spherical surfaces



Seongcheol Choi ^a, Rafael Vazquez-Duhalt ^b, Olivia A. Graeve ^{a,*}

- a Department of Mechanical and Aerospace Engineering, University of California, San Diego, 9500 Gilman Drive MC 0411, La Jolla, CA 92093-0411, USA
- ^b Centro de Nanociencias y Nanotecnología, Universidad Nacional Autónoma de México, Carretera Tijuana-Ensenada Km. 107, C.P. 22860, Ensenada, B.C., México

G R A P H I C A L A B S T R A C T



ARTICLE INFO

Article history:
Received 16 August 2021
Revised 10 January 2022
Accepted 11 January 2022
Available online 13 January 2022

Keywords:
Silica nanoparticles
L-lysine
Polystyrene particles
DLVO theory
Electrical double layer
Charge regulation

ABSTRACT

Hypothesis: We describe the deposition behavior of monodispersed silica nanoparticles on polystyrene spherical particles by using modified pairwise DLVO (Derjaguin-Landau-Verwey-Overbeek) interaction force profiles at pH values between two and twelve. Our modified model contains a new nonlinear charge regulation parameter that considers redistribution of ions, which allows us to realistically express the electrical double layer (EDL) interaction forces.

Experiments: Silanol-terminated silica nanoparticles $(7.6 \pm 0.4 \text{ nm})$, ι -lysine-covered silica nanoparticles $(7.8 \pm 0.4 \text{ nm})$, and polyallylamine hydrochloride-covered polystyrene (PAH/PS) particles $(348 \pm 1 \text{ nm})$ were synthesized. Then, each type of silica nanoparticle was deposited on the PAH/PS particles at a range of pH values.

Findings: Our new regulation parameter describes the realistic redistribution of charges governed by pH, total salt concentration, ionic strength of solution, and separation distance of particles. We find that this regulation parameter can be roughly approximated from the absolute values of theoretically calculated surface charge density and potential distributions, as well as experimentally measured ζ -potentials. Morphological analysis using electron microscopy of the experimental systems shows that the modified pairwise DLVO interaction forces exceptionally describe the deposition behavior of the silica nanoparticles physically adsorbed on the PAH/PS particle substrates.

© 2022 Elsevier Inc. All rights reserved.

^{*} Corresponding author.

E-mail address: ograeve@ucsd.edu (O.A. Graeve).

1. Introduction

The synthesis of organic/inorganic hybrid nanoparticles has been extensively studied for their applications in a variety of technologies, including battery systems, optics, biomedicine, and electronics [1-4]. For synthesis of these systems, it is typical for an inorganic material to be decorated on an organic substrate, resulting in countless variations for different sizes, shapes, and types of materials, and providing many options for the design of hybrid materials. Generally, there are four strategies to prepare organic/ inorganic hybrid nanoparticles, namely deposition of ex situ synthesized inorganic nanoparticles on a prepared organic substrate by either covalent or noncovalent bonding [2-3,5-8], in situ growth of inorganic nanoparticles by crystallization or precipitation on the polymer substrate [9-14], in situ synthesis of polymer particles in the presence of inorganic nanoparticles [15-18], and simultaneous synthesis of both polymer and inorganic nanoparticles [19-20]. The first strategy can result in controlled size and shape of both the organic and inorganic components. However, the deposited inorganic particles can undergo aggregation depending on the pH, ionic strength, and separation distance of the nanoparticles, among others. These aggregated particles become irreversibly bound and manifest behaviors of the aggregates instead of the behaviors of single inorganic nanoparticles. Thus, to gain control in such systems, the deposition behavior and surface interactions of the inorganic nanoparticles must be explored.

One can normally discuss the aggregation behavior of colloidal particles in terms of interaction energies or forces based on the classical theory developed by Derjaguin, Landau, Verwey, and Overbeek (DLVO) [21–23]. This theory assumes that particle interactions are mainly dominated by van der Waals (vdW) and electrical double layer (EDL) forces. EDL forces are described by the Poisson-Boltzmann theory, which states that surfaces in aqueous solutions maintain constant charge or constant potential, an unrealistic scenario for most cases [24]. In addition, the classic EDL model and its derivatives fail to effectively describe the interaction energy or force of asymmetric systems such as oppositely charged surfaces [25]. For isolated particles in dilute solutions, the surface charge density and surface potential are regulated by the adsorbed ions on the surfaces, total salt concentration, pH and ionic strength of the solution, inducing protonation and deprotonation of the ionizable chemical groups on the surfaces. In practical cases, the charged surface density and surface potential vary when the colloidal particles approach each other, as this triggers redistribution of ions on the surfaces. This phenomenon in which the surface charge density is controlled by the redistributed ions is called charge regulation [25-31].

Studies have used the linearized Poisson-Boltzmann model, which introduces a parameter to describe the charge regulation behaviors for both symmetric and asymmetric surfaces in solution [26-32]. In this model, symmetric surfaces are described as having the same charge densities or potentials, while asymmetric surfaces bear different charge densities or potentials. The model expresses charge regulation by assuming that the value of the regulation parameter remains constant when the two surfaces approach each other. This is called the constant regulation approximation and valid for situations in which there is low ionic strength and low potential. Its derivation originates from the linearized Poisson-Boltzmann equation and Debye-Hückel approximation [33]. Although this model has been considered a leap forward, an extended model to describe more complex situations is still unavailable. This may include systems having asymmetric particles, for example, an EDL interaction between a slightly charged amine-functionalized polymer particle and a fully charged silica nanoparticle at high pH. To efficiently describe practical cases like

this one, the EDL interaction force term should be governed by a charge regulation model that describes the redistribution of ions near the surface depending on pH, total salt concentration, ionic strength of solution, and separation distance.

In this study, we describe the deposition behavior of inorganic silica nanoparticles on oppositely charged submicron-sized polymeric particles, together with a generalized pairwise EDL interaction model that is valid for both symmetric and asymmetric cases. A regulation parameter as a function of pH and functional groups on particle surfaces is introduced for symmetric systems. Our analysis includes the development of (i) a nonlinear relationship between surface charge and surface potential under realistic charge regulation conditions and a nonlinear Poisson-Boltzmann model; and (ii) a method to find the diffuse layer potential by considering the diameter of the dominant ionic component near the surfaces. To compare and verify that our model effectively describes a wide range of practical cases, including low and high ionic strength solutions and low and high surface potentials, two different monodisperse silica nanoparticles, silanol-terminated silica nanoparticles and L-lysine-covered silica nanoparticles, and uniform-sized polyallylamine hydrochloride (PAH)-covered polystyrene (PS) particles, were experimentally prepared. For the case of the silanol-terminated silica nanoparticles, we scrutinize the vdW and EDL interaction forces for (1) two silanol-terminated silica nanoparticles (symmetric system) and (2) silanol-terminated silica nanoparticles on PAH/PS particles (asymmetric system). For the case of the L-lysine-covered silica nanoparticles, we scrutinize the vdW and EDL interaction forces of (3) two L-lysine-covered silica nanoparticles (symmetric system) and (4) L-lysine-covered silica nanoparticles on PAH/PS particles (asymmetric system). Since the calculated values used in our analysis correspond to the force between two particles of interest, if the concentration of the particles is high, these two particles will also interact with other particles in the same system, resulting in a significant deviation between the experimental results and theoretical model. Therefore, dilute solutions are used in this work to minimize the error between the experiment and the model [24–25]. Also, non-DLVO forces are ignored.

2. Experimental methodology

The procedure to prepare the PAH/PS particles covered with silanol-terminated silica nanoparticles [Figure SF1(a), page S2] or with ι -lysine-covered silica nanoparticles [Figure SF1(b), page S2] is illustrated in Supplementary Information.

Materials: Styrene (≥99%, contains 1% of 4-*tert*-butylcatechol as a stabilizer), potassium persulfate (≥99.0%), tetraethyl orthosilicate (TEOS, 98%), ι -lysine (≥98%), cyclohexane (99.5%, anhydrous), ammonium hydroxide solution (NH₄OH, 28.0–30.0%), ammonium chloride (NH₄Cl, ≥99.5%), hydrochloric acid (HCl, 37%), sodium hydroxide (NaOH, >98%, pellets), poly(allylamine) hydrochloride (PAH, M_w: 5,000–15,000 g/mol), and sodium chloride (NaCl, ≥99.5%) were purchased from Sigma-Aldrich (St. Louis, MO). All chemical reagents except styrene were used without further purification. Relevant pH adjustments for the solutions were controlled with either HCl or NaOH solutions. Deionized water was used for all experiments.

Synthesis of silanol-terminated silica nanoparticles: $NH_4Cl \cdot NH_3$ buffer solution of pH 9.0 was prepared by adding 10 mM NH_4Cl to 0.1 M NH_4OH solution. A volume of 350 mL of the $NH_4Cl \cdot NH_3$ buffer solution was heated to 60 °C in a round flask, and a mixture of TEOS (100 mL) and cyclohexane (50 mL) was added [34–35]. The solution was stirred vigorously for 24 h and then cooled to room temperature. The aqueous layer containing silanol-terminated silica nanoparticles on the bottom of the reactor was collected, fil-

tered with water of pH 6.5 by using an aluminum oxide filter membrane (pore size: 0.02 μ m, Anodisk, Whatman®, GE Healthcare, Chicago, IL), which has straight porous channels. Then, the filtered sample was diluted to 1.0×10^{-5} wt% with water of the same pH and redistributed by ultrasonication for 15 min. The pH of this solution was 6.7.

Synthesis of ι -lysine-covered silica nanoparticles: A mass of 28 mg of ι -lysine was dissolved in 28 mL of water in a reactor at 351 K. Then, 2.0 g of TEOS were injected into the mixture, and the mixture was vigorously stirred for 24 h and cooled to room temperature [36–39]. To remove the impurities (i.e., free ι -lysine and ethanol) the solution was filtered using an aluminum oxide membrane. The filtered sample was diluted to 1.0×10^{-5} wt% with water and redistributed by ultrasonication for 15 min. The measured pH of this solution was 7.3.

Synthesis of sulfate-terminated polystyrene particles: The styrene precursor was washed 4 times with a solution of 1.0 M NaOH to remove the 4-tert-butylcatechol inhibitor. Then, the washed styrene was dried with magnesium sulfate before use. The anionic polystyrene (PS) particles consisting of sulfate-ended chains were prepared by soap-free emulsion polymerization [40]. A mass of 10 g of purified styrene was vigorously mixed with 190 g of water in a three-necked flask for an hour under nitrogen atmosphere at 348 K. Then, 10 g of water containing 0.10 g of potassium persulfate were injected into the reactor to initiate the chain-growth polymerization and incubated for 24 h. The PS particle suspension was washed 7 times with excess water by a sequence of ultrasonication and centrifugation to eliminate impurities such as unreacted sulfate molecules, styrene monomers, dimers, and trimers. The concentration of the purified PS particle suspension was diluted to 0.10 wt% with water, and then the solution was mixed by ultrasonication for 15 min. The measured pH of this solution was 7.2.

Physisorption of PAH on sulfate-terminated PS particles: In order to coat a PAH monolayer on the sulfate-terminated PS particles, 1.0 mL of 20 wt% PAH water solution was poured into 30.0 mL of the 0.10 wt% PS particle suspension, and then the mixture was vigorously stirred for 24 h at room temperature [41–45]. The solution was microfiltered 5 times with excess water by using a cellulose acetate membrane filter (pore size: 0.20 μm , Advantec MFS, Inc., Dublin, CA) to remove free PAH molecules. The purified sample was diluted to 1.0×10^{-5} wt% with water, and the measured pH was 6.7.

Deposition of silica nanoparticles on PAH/PS particles: A 1.0 mL suspension of 1.0×10^{-5} wt% silica nanoparticles was incorporated into 10 mL of the PS particle solution and vigorously stirred for 10 s. Then, the pH of each mixture was adjusted to 2, 4, 6, 8, 10, and 12 with 0.1 mM of HCl solution to lower the pH or 0.1 mM of NaOH to increase the pH of each mixture. After mixing for 6 h at room temperature, each sample was microfiltered 3 times with water of the same pH by using a cellulose acetate membrane filter.

Characterization: A field emission scanning electron microscope (FE-SEM, Zeiss Sigma 500, Carl Zeiss AG, Oberkochen, Germany) and a transmission electron microscope (TEM, JEOL 1200 EX II, JEOL Ltd., Tokyo, Japan) were used to observe the morphology of the powders. A drop of suspension was placed on aluminum foil and dried in a vacuum oven at room temperature for a week to minimize the thermal effect on the pairwise EDL forces between all particles and to maintain the original morphology of the particles. Temperature is one of the controlling parameters of surface charge. If the sample is dried at higher temperature, charge redistribution occurs at the particle surfaces. The potential profile also changes and the modified value of the EDL force initiates the movement of the attached silica nanoparticles, changing the morphologies of the nanoparticles physically adsorbed on the PS parti-

cles. The samples for SEM were not sputter-coated since this may affect the original morphology of the silica nanoparticles. The hydrodynamic size distributions and the ζ -potentials of all the particle suspensions were measured using dynamic light scattering (DLS, Nanotrac Wave II, Microtrac, Inc., Montgomeryville, PA) [46–57]. All particle suspensions were ultrasonicated for 10 min before measurements using DLS.

3. Theoretical model

In this section, the modified pairwise DLVO interaction force model is discussed with the assumption that the total interaction force $[F_{DLVO}(D)]$ is a sum of the vdW force $[F_{vdW}(D)]$ and the EDL force $[F_{EDL}(D)]$:

$$F_{\text{DLVO}}(D) = F_{\text{vdW}}(D) + F_{\text{EDL}}(D) \tag{1}$$

where *D* is the separation distance between surfaces [21–23]. The vdW interaction force term between spheres used in this work was computed as described in Supporting Information (pages S3–S6). The modified EDL force model is valid for both symmetric and asymmetric spherical particles having low and high surface potentials, under low and high ionic strength of solutions at different pH values. In this study, the symmetric systems include solutions of silanol-terminated silica nanoparticles and *L*-lysine-covered silica nanoparticles and between two silanol-terminated silica nanoparticles. The asymmetric systems include mixed solutions of PAH/PS particles with silanol-terminated silica nanoparticles and PAH/PS particles with *L*-lysine-covered silica nanoparticles.

3.1. EDL interaction forces for symmetric and asymmetric systems

We introduce a regulation parameter p_i , based on the nonlinear Poisson-Boltzmann model, to the EDL interaction energy for either symmetric or asymmetric isolated plates. Then, these EDL energies are converted to EDL interaction forces between two spherical particles by using the Derjaguin approximation [25].

3.1.1. Nonlinear charge regulation relation between surface charge density and surface potential

Derivations of the charge regulation relations between the surface charge density and surface potential are presented in Supporting Information (pages S7-S12) for the silanol-terminated silica nanoparticles [Equation (SE13)], \(\lloar{\chi}\)-lysine-covered silica nanoparticles [Equation (SE19)], and PAH/PS particles [Equation (SE24)]. These charge regulation equations are still unrealistic because of the effects of total salt concentration and ionic strength of the solution, which also change as the pH of the solution is varied. Moreover, since both the surface charge density and surface potential are unknown in these equations, we need one more independent equation to solve the relation between surface charge density and surface potential at specific pH values.

The surface charge is regulated by proton concentration on the surface and by all co-ions and counter-ions in solution, which affects the charge balance within the EDL and changes the proton concentration profile. Thus, the second relation between surface charge density and surface potential should be dependent on total ionic concentrations on the surface. The well-known Poisson equation describes a Laplacian of the potential as a function of the distance \times away from the surface [25] and the ionic concentration profile $C_{x,i}$ as:

$$\nabla^2 \psi = \frac{\mathrm{d}^2 \psi}{\mathrm{d}x^2} = -\frac{z_i q C_{x,i}}{\varepsilon_0 \varepsilon_r} \tag{2}$$

where ε_o is the permittivity of vacuum and ε_r is the relative permittivity of water at room temperature. Since the ionic concentration follows a Boltzmann's distribution, one can combine Equation (SE4) in Supplementary Information and Equation (2), resulting in the Poisson-Boltzmann equation [25]:

$$\frac{\mathrm{d}^2 \psi}{\mathrm{d}x^2} = -\frac{q N_{\mathrm{A}}}{\varepsilon_{\mathrm{o}} \varepsilon_{\mathrm{r}}} \sum_{i} z_i C_{\infty,i} e^{\frac{z_i q \psi_{\mathrm{x}}}{k_{\mathrm{B}} T}} \tag{3}$$

This Poisson-Boltzmann equation governs the electrostatic potential distribution for a charged surface, which is immersed in an electrolyte solution [58–61]. From Equation (3), the Grahame equation is obtained [25]:

$$\sigma = \sqrt{8\varepsilon_{o}\varepsilon_{r}k_{B}TN_{A}C_{\infty} \times 10^{3}} \sinh\left(\frac{q\psi_{o}}{2k_{B}T}\right) \tag{4}$$

This equation shows that there is, indeed, a second relation between surface charge density and surface potential, which depends on the total concentration of salts C_{∞} . All the variables required to compute values for this relation are listed in Table ST3 (page S13 of Supplementary Information).

By using the optimize.root() function from the SciPy package of Python, the solution of each pH-dependent charge regulation model [Equations (SE13), (SE19), and (SE24) in Supplementary Information] and the Grahame equation [Equation (4)] results in a pair of roots of σ and ψ_o with respect to pH of the solution for each symmetric surface. These relations between surface charge density and surface potential are valid for isolated surfaces and both low and high potential cases because the Grahame equation is based on a nonlinear Poisson-Boltzmann equation. However, the ionic strength of the solution is not considered in this model. Moreover, this charge regulation model does not describe the changes in surface charge density and surface potential for the two surfaces upon approach. Therefore, we should introduce a regulation parameter under this nonlinear charge regulation relation so that both the surface charge density and the surface potential are affected by the ionic strength of the solution and the separation distance.

3.1.2. Regulation parameter

For large separations ($D \to \infty$), a local linearization of the charge and potential relation permits an arbitrary value and approximation of p(D) [26,32]:

$$p_i = \lim_{D \to \infty} P_i(D) = \frac{C_{\text{dl},i}}{C_{\text{dl},i} + C_{\text{in},i}}$$

$$(5)$$

where p_i is the regulation parameter for plate i, $C_{\text{dl},i}$ is the diffuse layer capacitance of the plate i, and $C_{\text{in},i}$ is the inner layer capacitance of plate i (described on page S14 of Supplementary Information). When the surface charge of two particles approaching each other is constant, then p(D) = 0; when the surface potential of two particles approaching each other remains constant, then p(D) = 1. Thus, the constant regulation approximation allows one to describe the charge regulation behavior of two surfaces approaching each other with a single arbitrary regulation parameter between 0 and 1 [21–22,26–32]. This regulation parameter depends on the capacitance within the Stern layer of the EDL [29]. The diffuse layer capacitance is obtained from:

$$C_{\text{dl},i} = \frac{\partial \sigma_{\text{dl},i}}{\partial \psi_{\text{dl},i}} = \varepsilon_0 \varepsilon_r \kappa \cosh\left(\frac{q \psi_{\text{dl},i}}{2k_B T}\right) \tag{6}$$

where $\psi_{\text{dl},i}$ is the diffuse layer potential at the outer Helmholtz plane. The location of the outer Helmholtz plane is determined using a straightforward definition by Stern [62]:

$$\delta = 2r_{\text{water}} + r_{\text{hydrated ion}} \tag{7}$$

where δ is the distance at the outer Helmholtz plane away from the surface, $r_{\rm water}$ is the radius of a water molecule (0.138 nm), and $r_{\rm hydrated~ion}$ is the radius of the dominant counter-ions near the isolated surface. The radii of hydrated ions [25] used are listed in Table ST4 of Supplementary Information (page S14). Once the co-ion and counter-ion profiles are known from the Boltzmann equation [Equation (SE4) in Supplementary Information], one can determine the dominant counter-ions near the solid/liquid interface, as listed in Table 1.

Now, we need the potential profile as a function of the distance \times to calculate the diffuse layer potential. For a monovalent electrolyte, the potential profile $\psi_{x,i}$ at a distance \times away from the surface is defined as [25]:

$$\psi_{x,i} = \frac{2k_BT}{q} \ln \left[\frac{1 + \left\{ tanh\left(\frac{q\psi_{o,i}}{4k_BT}\right) \right\} e^{-\kappa x}}{1 - \left\{ tanh\left(\frac{q\psi_{o,i}}{4k_BT}\right) \right\} e^{-\kappa x}} \right]$$
 (8)

where κ is the inverse Debye screening length defined by [25]:

$$\kappa = \sqrt{\frac{\sum_{i} q^{2} Z_{i}^{2} C_{\infty,i} N_{A} \times 10^{3}}{\varepsilon_{o} \varepsilon_{r} k_{B} T}}$$

$$(9)$$

The potential profile of Equation (8) is governed by the surface potential based on the nonlinear charge regulation relation and the ionic strength of the solution. With the given conditions, δ is incorporated as \times into Equation (8) to find the diffuse layer potential $\psi_{dl,i}$ of plate i.

3.1.3. Generalized EDL interaction force

An integration over the separation distance yields the pairwise EDL interaction energy between two plates i and j:

$$W_{\text{EDL,planes}}(D) = \int_{D}^{\infty} \prod_{j}(D') dD' =$$

$$= \varepsilon_{0} \varepsilon_{r} \kappa \frac{2\psi_{o,i}\psi_{o,j} e^{-\kappa D} + \left[(2p_{i}-1)\psi_{o,j}^{2} + (2p_{j}-1)\psi_{o,i}^{2} \right] e^{-2\kappa D}}{1 - (2p_{i}-1)(2p_{j}-1) e^{-2\kappa D}}$$
(10)

where p_i and p_j are the regulation parameters of two different plates, i and j, respectively [22,33]. Even though Equation (10) is originally derived from the linearized Poisson-Boltzmann equation within the Debye-Hückel approximation, the EDL interaction energy is affected by the regulation parameter based on a nonlinear charge-potential relation. Thus, Equation (10) indeed describes the EDL interaction energy of either symmetric or asymmetric plates with realistic charge regulation behaviors, which are determined by pH, total concentration of salts, ionic strength of the electrolyte solution, and the separation distance. This model is also valid for low to high ionic strength of the solution and low to high surface potential cases. The EDL interaction force $F_{\text{EDL,spheres}}(D)$ between two spheres can be obtained by the Derjaguin approximation:

$$F_{\rm EDL, spheres}(D) = 2\pi \, \frac{R_i R_j}{R_i + R_j} \, W_{\rm EDL, planes}(D) \tag{11} \label{eq:edl_fit}$$

By incorporating the vdW force from Equation (2) and the EDL force from Equation (11) into Equation (1), the pairwise DLVO interaction force profiles as a variation of pH are obtained for either symmetric or asymmetric spheres. What we are interested in are the force profiles for the two different asymmetric cases: (i) a silanol-terminated silica nanoparticle and a PAH/PS particle and (ii) an ι -lysine-covered silica nanoparticle and a PAH/PS particle. Thus, the regulation parameters and the surface potential values for all three symmetric surfaces are required as defined in Equation (10). Additional variables required to compute the regulation parameters of plate i and the EDL interaction force between two particles are listed in Table ST5 (page S15 of Supplementary Infor-

Table 1Dominant counterion species and distance at outer Helmholtz plane away from the surface of a particle with respect to pH of solution.

pН	Silanol-terminated silica nanoparticles		ι-lysine-covered silica nanoparticles		PAH/PS particles	
	Dominant counterions (a)	δ (nm) (b)	Dominant counterions (a)	δ (nm) (b)	Dominant counterions (a)	δ(nm) (b)
2	Cl-	0.61	CI-	0.61	Cl-	0.61
4	H ⁺	0.56	Cl ⁻	0.61	Cl-	0.61
6	H ⁺	0.56	H ⁺	0.56	Cl-	0.61
8	Na ⁺	0.63	Na ⁺ , H ⁺	0.61 ^(c)	OH ⁻	0.66
10	Na ⁺	0.63	Na ⁺	0.63	OH ⁻	0.66
12	Na ⁺	0.63	Na ⁺	0.63	OH ⁻	0.66

⁽a) Dominant counterion species at outer Helmholtz plane.

mation). The entire calculation procedure of this work is diagrammatically represented in Figure SF2 (page S16 of Supplementary Information).

3.2. Summary of model contributions

The most recent regulation parameter model is based on a simple charge regulation effect with constant regulation under the Debye-Hückel approximation [21–22,28–29,31,61]. It makes use of a mathematical relationship between the regulation parameter and the diffuse layer potential, with values that can be determined by direct measurements of the pairwise interaction force and capacitances $C_{\rm dl}$, $C_{\rm in}$, $C_{\rm bi}$, and $C_{\rm s}$ [29]. For computational simplicity, the Grahame equation is used based on a direct relationship between surface charge density and diffuse layer potential, instead of surface potential. Even though this approach agrees well with experimental results, it has limitations to appropriately describe realistic charge regulation behaviors of a larger variety of colloidal systems.

To properly estimate the pairwise EDL interaction forces under realistic charge regulation behaviors for more practical cases, our proposed model introduces a mathematical procedure to determine the regulation parameter without any experimental measurements. To improve the regulation parameter model, our contributions include (i) a nonlinear relationship between surface charge and surface potential based on the charge regulation effect occurring over a wide range of pH values using nonlinear Poisson-Boltzmann theory, and (ii) a method to define the diffuse layer potential by considering the size of dominant ionic species near surfaces.

First, we show the nonlinear relation between surface charge and surface potential for all possible equilibrium acid-base reactions of a single functional group and multi-functional groups on the surfaces of particles in the pH range from 2 to 12. This method is valid for more practical situations such as low to high pH and low to high electrolyte concentration. Second, considering the size of dominant ions near surfaces allows us to define the diffuse layer potential in the outer Helmholtz plane. The values (surface charge density, surface potential, and diffuse layer potential) determined by these two methods are used to find the regulation parameters, which describe the pairwise EDL interaction forces of particles under a realistic charge regulation effect. If the concentration of particles in solution is dilute, this generalized EDL interaction force model is valid for low to high pH, low to high electrolyte concentration, single to multi-functional surface groups, symmetric systems, and asymmetric systems. This is because the primary assumption of the mathematical description of the pairwise interaction force is that the two interacting particles are not under any external forces [25].

4. Results and discussion

An appropriate theoretical description of the interaction energies and forces for particles in suspension, which includes effects

associated with particle morphologies and surface chemistry, is crucial to avoid a significant deviation from real results [23]. First, both the vdW and EDL terms depend on geometry of the particles, which can be defined by size, shape, surface roughness, and density. Particularly, the surface roughness must not be ignored for the vdW interaction term since the strength of this interaction extends meaningfully from 0.2 to 1 nm away from the surface [23,63–66]. For example, surface roughness of spherical particles greater than 1 nm causes uneven vdW interactions between the surface of a sphere and that of another sphere, resulting in a drastic decrease in the pairwise vdW interaction. Second, a deep understanding in protonation and deprotonation of the functional groups on the surface of the colloidal spheres allows defining how many specific chemical groups are ionized and contribute surface charge density at a given pH and ionic strength. Thus, to justify that all the colloidal particles used in this work are ideal for our theoretical model, morphological studies using electron microscopy techniques are presented in Supporting Information (pages S17-S26).

4.1. Nonlinear charge regulation relationship between surface charge density and surface potential

In this section, we analyze the changes in both surface charge density and surface potential with respect to pH from the perspective of Boltzmann's distribution of each ionic species on the surface. Surface charge density and surface potential are computed by the charge regulation equations [Equations (SE13), (SE19), and (SE24) in Supplementary Information] and the Grahame equation [Equation (4)] and plotted in Fig. 1. The raw data for this figure is available in Table ST6 in Supplementary Information (pages S27-S29). Fig. 1(a) shows the surface charge density of the silanolterminated silica nanoparticles, L-lysine-covered silica nanoparticles, and PAH/PS particles with respect to pH. Fig. 1(b) presents the same information with reduced axes for clarity at small values. To discuss further the surface charge density behaviors of these colloidal particles, we explore the shifts of the ionic concentrations in log scale between the bulk solution and the solution on the surface of each particle as a variation of pH, as displayed in Fig. 2 (raw data information available on page S30 of Supplementary Information). In this figure, we compare the changes in the bulk ionic concentration of each species [Fig. 2(a)] with the changes in each ionic concentration on the surface of the silanol-terminated silica nanoparticles [Fig. 2(b)], the *i*-lysine-covered silica nanoparticles [Fig. 2(c)], and the PAH/PS particles [Fig. 2(d)]. Each ionic concentration on the surface is computed using the Boltzmann equation [Equation (SE4) in Supplementary Information] with the calculated surface potential. Each plot is divided into several regions depending on changes in the slope of the ionic concentration with respect

Surface charge density of silanol-terminated silica nanoparticles: As seen in Fig. 1(a), at pH 2 the surface of the silanol-terminated silica nanoparticles is very slightly positive (+0.17 μ C/m²) because a few protonated silanol groups bear positive charge and most of

⁽b) Distance at the outer Helmholtz plane away from the surface of a particle.

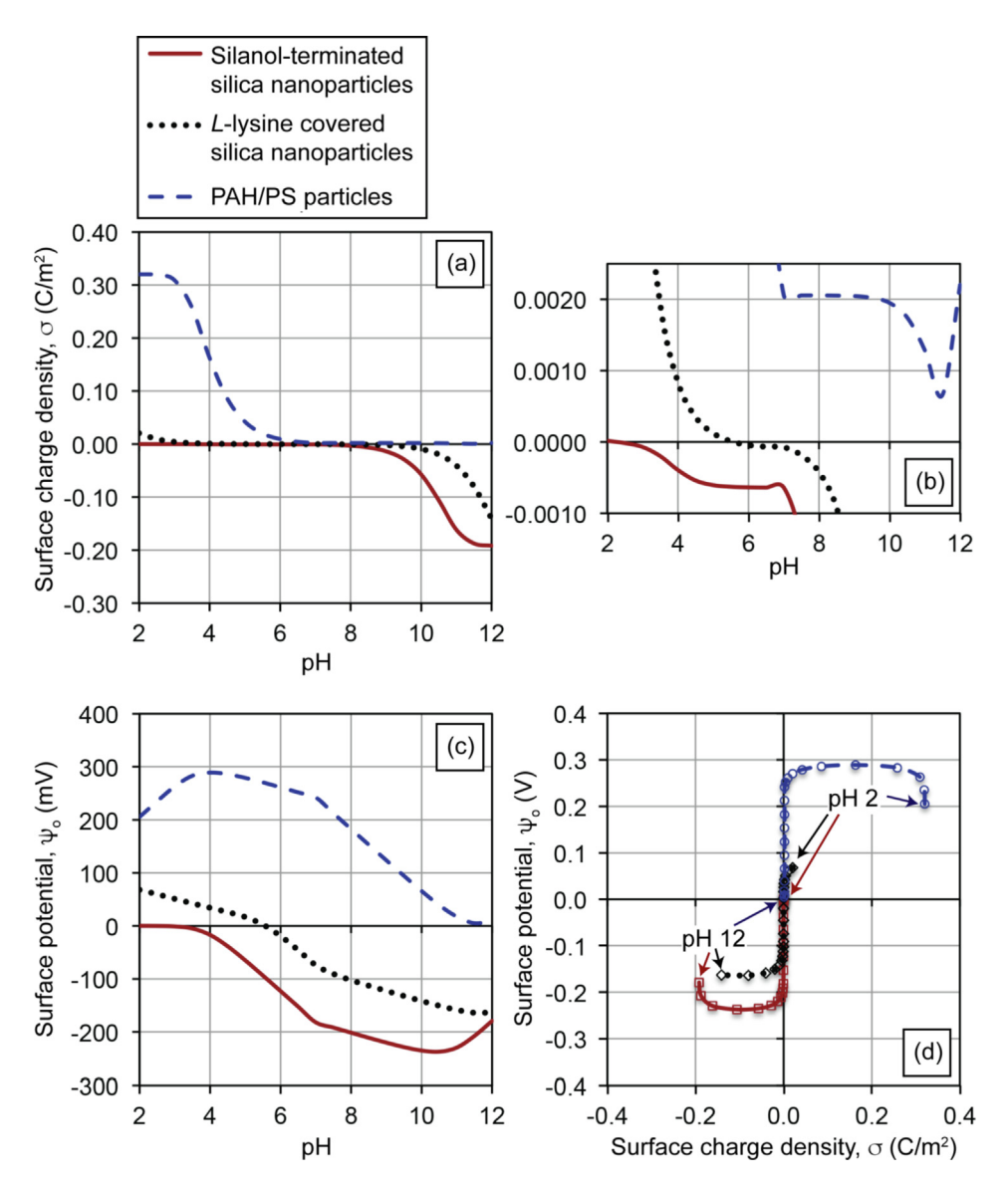


Fig. 1. (a)-(b) Surface charge density profiles as a function of pH, (c) surface potential as a variation of pH, and (d) surface charge density versus surface potential for silanol-terminated silica nanoparticles, ι-lysine-covered silica nanoparticles, and PAH/PS particles.

the silanol groups are neutral due to high concentration of protons in the solution. At pH between 2.0 and 2.5, there is a charge inversion from slightly positive to slightly negative with an increase in pH [Fig. 1(b)]. Region I of Fig. 2(b) shows that the ionic concentration on the surface is very similar to the behavior shown in Fig. 2(a) at the same pH range (i.e., from 2 to 4) for $[H^+]_0$, $[Cl^-]_0$, and $[OH^-]_0$. In both figures, the value at pH 2 is the same and the slopes of all three curves point in the same direction for each of the ionic species. This is expected because the rates of change of $[H^+]_0$, $[Cl^-]_0$, and $[OH^-]_0$ on the surface with respect to pH are very close to that of each bulk ionic concentration of the $[H^+]_{\infty}$, $[Cl^-]_{\infty}$, and $[OH^-]_{\infty}$, as seen by comparing Fig. 1(a) and 2(b). Referring to Fig. 1(a) from pH 4 to 7, the surface charge density is constant even though the concentration of protons $[H^+]_{\infty}$ in the solution, which decreases with increase in pH, is much lower at pH 7 compared to pH 4. Region II of Fig. 2(b) shows that the ionic concentration profiles on the surface do not follow the bulk ionic concentration profiles, shown in Fig. 2(a), between pH 4 and 7. In region II, an increase in pH does not change [H⁺]₀ and [OH⁻]₀, whereas in the bulk the ionic concentration of [H⁺]₀ decreases and that of [OH⁻]₀ increases with increasing pH. Because the density of SiO $^-$ on the silica surface does not change from pH 4 to 7 in Fig. 1(a), the concentration of the only counterion, H $^+$, on the silica surface in Region II of Fig. 2(b) must be constant as well. If $[H^+]_0$ is constant, $[OH^-]_0$ must also be constant, since the auto-ionization of water molecules obeys pH + p OH = 14 everywhere in the aqueous solution at room temperature. We refer to this as the buffer capacity (*i.e.*, the capacity to protect the volume close to the surface from changes in ionic concentration of protons and hydroxide anions on the surface). On the other hand, $[CI^-]_0$ changes sensitively by the change in pH to meet local charge balance, which shows that this ionic species is not buffered.

From pH 7 to 11 in Fig. 1(a), as additional NaOH is added to the solution, there is an increase in the absolute value of the surface charge density of the silanol-terminated silica nanoparticles (*i.e.*, the surface charge density becomes more negative). Since this negative surface charge density is high enough to strongly attract more protons and sodium cations near the surface, $[H^+]_0$ and $[Na^+]_0$ show shifts to higher concentrations when comparing the bulk concentrations in Fig. 2(a) with those on the surface in Fig. 2(b). Above pH 11, the surface charge density reaches its max-

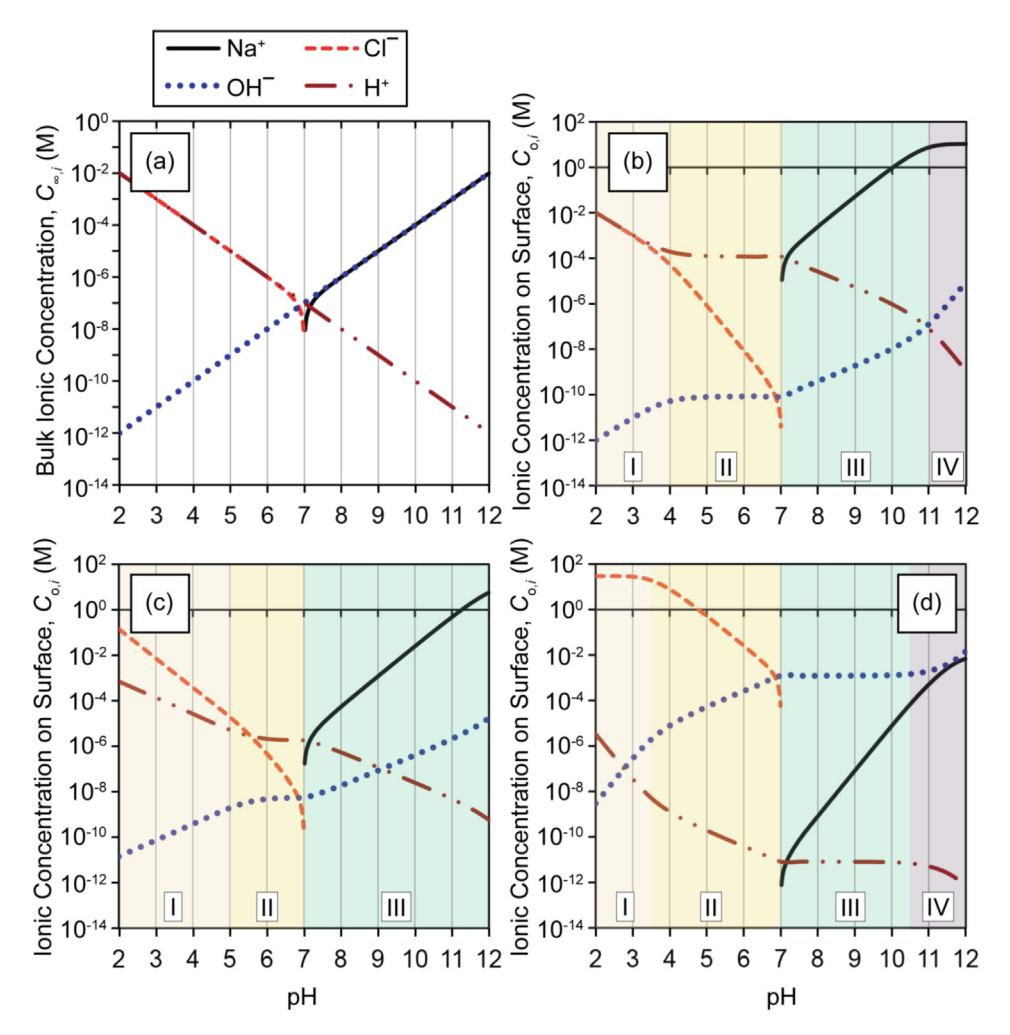


Fig. 2. Concentration profiles of sodium ions, hydroxide ions, chloride ions, and protons with respect to pH from acidic to basic for (a) bulk solutions, (b) on the surface of silanol-terminated silica nanoparticles, (c) on the surface of *ι*-lysine-covered silica nanoparticles, and (d) on the surface of PAH/PS particles.

imum (negative) value, which means that all the silanol groups on the surface are fully deprotonated and exert the maximum charge. As plotted in region IV of Fig. 2(b), $[\mathrm{Na^+}]_0$ is constant above pH 11. Although more NaOH is added into the solution, the surfaces of the silanol-terminated silica nanoparticles do not accept more sodium cations. Instead, more sensitive changes of $[\mathrm{H^+}]_0$ and $[\mathrm{OH^-}]_0$ are the source of the surface buffer capacity of this sodium ion.

Surface charge density of L-lysine-covered silica nanoparticles: In Fig. 1(a), the surface charge density of the L-lysine-covered silica nanoparticles is weakly positive between pH 2 to 5. This is because the surface contains more $\alpha - NH_3^+$ than α - COO^- in this acidic environment. Thus, this weakly positive surface charge slightly repels protons and attracts more chloride anions and hydroxide ions near the surface. As seen in region I of Fig. 2(c), compared to the bulk ionic concentration distributions in Fig. 2(a), a shift of [H⁺]₀ to a lower concentration and shifts of [Cl⁻]₀ and [OH⁻]₀ to higher concentrations support these ion redistributions. Fig. 1(b) shows that the surfaces of the *L*-lysine-covered silica nanoparticles undergo a charge inversion from slightly positive to very weakly negative between pH 5 and 6. This indicates that the number of α - COO^- starts slightly exceeding that of α - $NH_3^{\ +}$ in this pH range. However, the overall numbers of both are almost equal. As seen in region II of Fig. 2(c), both [H⁺]₀ and [OH⁻]₀ are almost constant, even when their bulk concentrations $[H^+]_{\infty}$ and $[OH^-]_{\infty}$, change by two orders of magnitude. Instead, [Cl⁻]₀ changes rapidly,

contributing to the buffer capacity for $[H^+]_0$ and $[OH^-]_0$ near the surface in region II. This indicates that both α - NH₂⁺ α - COO on the surface of the *L*-lysine-covered silica nanoparticles are fully ionized and do not accept or lose more protons in this pH range. Incorporation of further NaOH into the solution causes an increase in the negative surface charge density of the L-lysine surface above pH 7, as depicted in Fig. 1(b). At pH 10, as seen in Fig. 1 (a), the surface charge density shows a drastic negative increase. This implies that the α - NH_3^+ starts becoming deprotonated, transitions to α -NH₂, and loses charge in basic conditions, while the α - COO⁻ stays constant without gain or loss of single protons (this will be discussed further at the end of this sub-section). At high pH, the surface bears enough negative charge density to attract protons and sodium ions and to repel the hydroxide ion. This is supported by the shifts of both $[H^+]_0$ and $[Na^+]_0$ to higher concentrations and the shift of $[OH^-]_0$ to lower concentration as represented in region III of Fig. 2(c), compared to the bulk ionic concentration in Fig. 2(a). The deviations between the ionic concentrations on the surface and the bulk ionic concentrations become larger with an increase in pH.

Surface charge density of PAH/PS particles: As seen in Fig. 1(a), the surface charge density of the PAH/PS particles is highly positive and constant between pH values of 2 to 3.5. This strongly charged positive surface attracts large amounts of both anionic species of chloride ions and hydroxide ions. Compared to the bulk ionic con-

centrations in Fig. 2(a), large shifts of these two ionic concentrations are seen in region I of Fig. 2(d). At pH 3.5, $[\text{Cl}^-]_0$ and $[\text{OH}^-]_0$ are 10^5 times higher than $[\text{Cl}^-]_\infty$ and $[\text{OH}^-]_\infty$, respectively. In addition, because this strong positive surface charge pushes the protons away from the surface, the magnitude of $[\text{H}^+]_0$ is only 10^{-5} of that of $[\text{H}^+]_\infty$ at the same pH. The plateau of the surface charge density between pH 2 and 3.5 in Fig. 1(a) indicates that all the amine groups are fully ionized and do not undergo protonation or deprotonation regardless of pH change. In Fig. 2(d), $[\text{Cl}^-]_0$ is constant from pH 2 to 3.5, while $[\text{H}^+]_\infty$ declines from 0.01 M to 3.16 \times 10^{-4} M in the same pH range. Instead, the sensitive changes of $[\text{H}^+]_0$ and $[\text{OH}^-]_0$ with respect to changes in pH are the source of the buffer capacity of these chloride anions on the surface.

Returning to Fig. 1(a), there is a drastic drop in the surface charge density from pH 3.5 to 7. This indicates that the NH₂+ groups begin deprotonation along with a decrease in the concentration of [H⁺]₀ as described in region II of Fig. 2(d). As seen in Fig. 1(b), from pH 7 to 10.5, the surface charge density of the PAH/PS particles is very weakly positive and constant regardless of change in pH. In Fig. 2(d), $[H^+]_0$ and $[OH^-]_0$ are also constant in this pH range due to the surface buffer capacity. Instead of changes in these concentrations on the surface, [Na⁺]₀ changes more sensitively to obey local charge balance near the surface in region III of Fig. 2(d). From Fig. 1(b) at pH 10.5, the surface charge density further decreases and finally reaches a minimum value of 6.58×10^{-1} ⁴C/m² at pH 11.5. From pH 11.5 to 12, the surface charge density slightly increases to 2.20×10^{-3} C/m², and from region IV of Fig. 2 (d), the change in each ionic concentration on the surface follows that of the bulk ionic concentration. This can be attributed to the almost neutral surface, which does not effectively attract the counterions or repel the co-ions and is barely involved in charge regulation.

Surface potential of silanol-terminated silica nanoparticles: From Fig. 1(c), the surface potential of the silanol-terminated silica nanoparticles from pH 2 to 4 is nearly zero because the surface charge density [see Fig. 1(a)] in this pH range is also very close to zero [67]; and because the high ionic strength of the solution screens the electric field between the silica nanoparticles, nullifying the surface potential. In the pH range from 4 to 7, the magnitude of this negative surface potential increases, even though the negative surface charge density is still extremely weak and constant., since the system contains much less ionic strength due to a lower concentration of pH-modifying salts. For an example of the system containing the silica nanoparticles at pH 7 without any additional salts, the Debye length is nearly 1 μ m [25] due to the very weak ionic strength of the solution, which means that the surface potential of this system is barely suppressed by electric field screening. Thus, the surface potential of the silica nanoparticles in the pH between 4 and 7 depends highly on the concentration of salts. Above pH 7, the strength of the surface potential keeps increasing, although a decrease in the ionic strength of the solution contributes to the shrinkage of the Debye length. More specifically, the surface potential from pH 7 to 9 is unexpectedly high, although the negative surface charge density in this pH range is still low. This is because the ionic concentration to screen the electric field between the silica nanoparticles is low in this pH range. From pH 9 to 11, the surface potential increases linearly compared to the large increase in surface charge density from 1.35×10^{-2} to 0.162 C/m². We can expect that in this pH range the increased concentration of ions causes effective electric field screening between the silica nanoparticles. At pH 11, the surface charge density does not increase any further because all the silanol groups are fully deprotonated. Above pH 11, the surface potential starts decreasing within the narrowed Debye length from 9.6 nm at pH 11 to 3.0 nm at pH 12 due to the high concentration of salts.

Surface potential of L-lysine-covered silica nanoparticles: As depicted in Fig. 1(c), the positive surface potential of the L-lysinecovered silica nanoparticles decreases from pH 2 to 5.5 and reaches zero at pH 5.5 [68]. This is because more α -carboxyl groups of the L-lysine shell become deprotonated with an increase in pH. There is a surface potential inversion from slightly positive to negative near pH 5.5, and a subsequent drastic increase of the negative surface potential from pH 5.5 to 7, while the surface charge density of the ι -lysine-covered silica nanoparticles in Fig. 1(a) is constant in this same pH range. Above pH 7, the α - NH₃⁺ groups start becoming deprotonated with an increase in pH, and the surface exhibits stronger negative charge. This mainly contributes to the increasing negative trend of the surface potential of the ι-lysine-covered silica nanoparticles above pH 7, especially the shallower slope of the surface potential profile above pH 11 that is mainly caused by the strong ionic strength of the solution.

Surface potential of PAH/PS particles: The strong positive surface charge of PAH/PS particles contributes to their high surface potential value between pH 2 and 4 as plotted in Fig. 1(c). Because the ionic strength of the solution is reduced to 1/100 from pH 2 to 4, the electric field reaches further with much less attenuation between the PAH/PS particles. As a result, the surface potential increases and reaches its maximum value at pH 4. The positive surface potential decreases with an increase in pH from 4 to 7 mainly because of a sharp drop of the surface charge density. From pH 7 to 10, although the surface charge density is constant, the surface potential keeps decreasing due to an increase in the ionic strength of the solution. Above pH 11, the surface potential approaches zero because the surface charge is also zero. The trend of the computed surface potential profile for each colloidal system with a variation of pH in Fig. 1(c) is the same as that of our experimentally measured zeta potential profile of each sample in Fig. 3. Because the ζ-potential should be proportional to the surface potential, this comparison between the computed surface potential profiles and experimentally measured ζ-potential plots validates our nonlinear charge regulation relation between surface charge density and surface potential. Detailed explanation of this comparison is provided in Supporting Information (pages S31-S32).

For each of the three colloidal systems, Fig. 1(d) shows the relationship between the surface charge density and the surface potential. Since these results are based on the nonlinear Poisson-Boltzmann and Grahame equations, the profiles generally behave non-linearly and we can specify the surface charge densitysurface potential relation as linear or nonlinear depending on the pH and the functional groups on the colloidal surface. First, the σ and ψ_0 profile of the silanol-terminated silica nanoparticles is linear from pH 2 to 7 and nonlinear from pH 7 to 12. Second, the profile of the L-lysine-covered silica nanoparticles with the amphoteric surface of amine groups and carboxyl groups shows a nonlinear relation from pH 2 to 4, a linear relation from pH 4 to 9, and a nonlinear relation from pH 9 to 12. Third, the profile of the aminefunctionalized PAH/PS particles exhibit a nonlinear relation from pH 2 to 7, which becomes linear between pH 7 to 12. For monovalent 1:1 electrolyte systems, such as the ones described in this work, for pH ranges where the σ and ψ_0 profiles behave linearly, the colloidal systems have a constant surface charge density and show a drastic change in the surface potential. When the behavior of σ and ψ_o is nonlinear, the surface potential changes along pH less sensitively than the surface charge density. Further discussions on how the ionizable surface is regulated by ionic concentrations are explained in terms of fractional composition distributions at different pH values in Supporting Information (pages S33-S39).

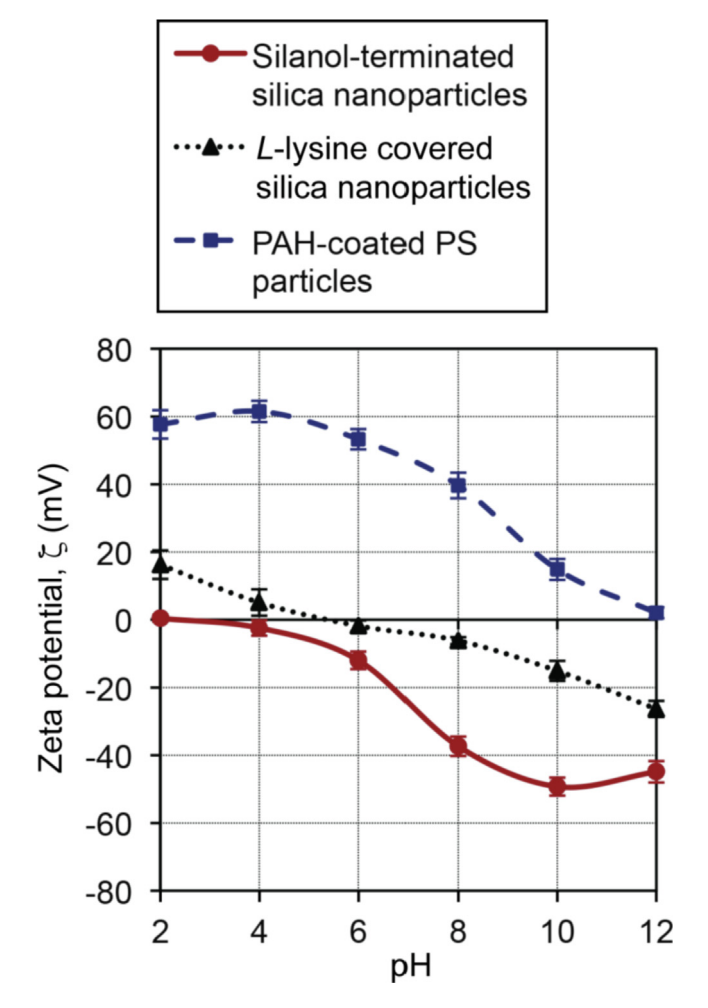


Fig. 3. Zeta potential profiles as a change of pH for silanol-terminated silica nanoparticles, *ι*-lysine-covered silica nanoparticles, and PAH/PS particles.

4.2. Regulation parameter under nonlinear charge regulation relation

As discussed in section 3, to define the regulation parameter under nonlinear charge regulation for each material, the diffuse layer potential at the outer Helmholtz plane should be determined [69-70]. Fig. 4(a) illustrates how the dominant ionic species, Na+ and OH-, are distributed away from the isolated silanolterminated silica nanoparticles at pH 12. Fig. 4(b) depicts the EDL structure at pH 12 in terms of the potential profile and the dominant counterion (Na⁺) concentration profile away from the surface of the silanol-terminated silica nanoparticles. The potential profile is plotted by using Equation (8) with the computed values of $\psi_{o.sil}$ ica from the data of Fig. 1(c) and κ from Equation (9). The counterion (Na+) concentration distribution is created by using Boltzmann's equation [Equation (SE4) in Supplementary Information]. The designated inner Helmholtz plane (0.134 nm), outer Helmholtz plane (0.560 nm), and Debye length (3.05 nm) are theoretically determined, and the shear plane (2.58 nm) is determined from the empirically measured ζ-potential value (Fig. 3). From Fig. 4(b), the potential distribution of a charged silica nanoparticle in a solution with high salt concentration tends to drop drastically within 1 nm from its surface due to a thin Debye length caused by high ionic strength. Because this case indicates that even a 0.1 nm difference in the outer Helmholtz plane location results in a large deviation in the diffuse layer potential, the accurately determined outer Helmholtz plane location for every case guarantees a reliable regulation parameter value.

As depicted in Fig. 4(b), the position of the outer Helmholtz plane is a sum of the diameter of the water molecule layer and the radius of the hydrated counterion [Equation (9)]. The dominant counterions near the surfaces of the silanol-terminated silica nanoparticles, the *i*-lysine-covered silica nanoparticles, and the PAH/PS particles at pH 2, 4, 6, 8, 10, and 12 are determined from Fig. 2(b), (c), and (d), respectively. These dominant counterions and the outer Helmholtz plane locations are summarized in Table 1. The outer Helmholtz plane locations are used to calculate the diffuse layer potentials to obtain the regulation parameters. For pH 2, 4, 6, 8, 10, and 12, the potential distributions of the isolated silanolterminated silica nanoparticles [Figure SF10(a)-(c)], the L-lysinecovered silica nanoparticles [Figure SF10(d)-(e) and the PAH/PS particles [Figure SF10(f)-(g) in] are provided in Supplementary Information (page S40). For the ionic concentration distributions as a function of the distance away from the surface, we provide only the case of the silanol-terminated silica nanoparticles at each pH, illustrated in Figure SF11 (pages S41-S42 in Supplementary Information).

The nonlinear relation between the surface charge density and the surface potential in Fig. 1(d) is valid for isolated surfaces such as in an extremely dilute solution. This limited charge regulation model only considers pH and total salt concentration. In real situations, the separation distance between immersed surfaces varies by interparticle interactions and Brownian motion. This indicates that the charge regulation model, which only considers pH and total salt concentration, fails to describe the realistic behaviors of the surface charge density and the surface potential of the approaching particles. When the separation distance decreases, the modified electric field triggers redistribution of ionic concentration near surfaces to obey the local charge neutrality between the surfaces. These repositioned ions force the changes in acidbase equilibrium of the surface functional groups, and this protonation or deprotonation causes a change in surface charge density as well as potential profile, including surface potential. This changed potential profile between the particles directly alters the electric field between them. As a result, the sum of the force from this modified electric field and vdW force primarily determines the next movements of the two colloidal particles. The cycle of these consecutive events occurs continuously until the system reaches thermodynamic equilibrium. Thus, if we can mathematically explain how both surface charge density and surface potential of the approaching particles behave, we will more accurately predict the behaviors of most practical colloidal particles of both symmetric and asymmetric systems.

A regulation parameter is a key tool to describe how both the surface charge and the surface potential change upon approach of the two surfaces [21-22]. Fig. 5(a) presents the variation of regulation parameter profiles obtained from Equations (5), (6), (SE25), (SE26), and (SE27). When the system has a p_i value of unity, the surface charge density of the particle surface is constant regardless of the redistribution of charges when the two particles are moving closer to each other. In contrast, the surface potential is constant for a p_i value of zero. However, the system with p_i = 1 or 0 is unrealistic because the redistribution of ions must occur for particles that are approaching. In most realistic situations, the surface charge density and the surface potential are not constant when the separation distance approaches zero. Thus, the regulation parameter value should be between 1 and 0. We discuss how p_i changes for each symmetric system with respect to pH and generalize this phenomenon.

The behavior of the regulation parameter in the silanol-terminated silica nanoparticles is categorized into four regions along pH, from 2 to 4, 4 to 7, 7 to 11, and 11 to 12. These pH ranges are the same as we defined for ionic concentration profiles in Fig. 2 (b). In the pH range from 2 and 4, p_i is 0.22 at a surface charge den-

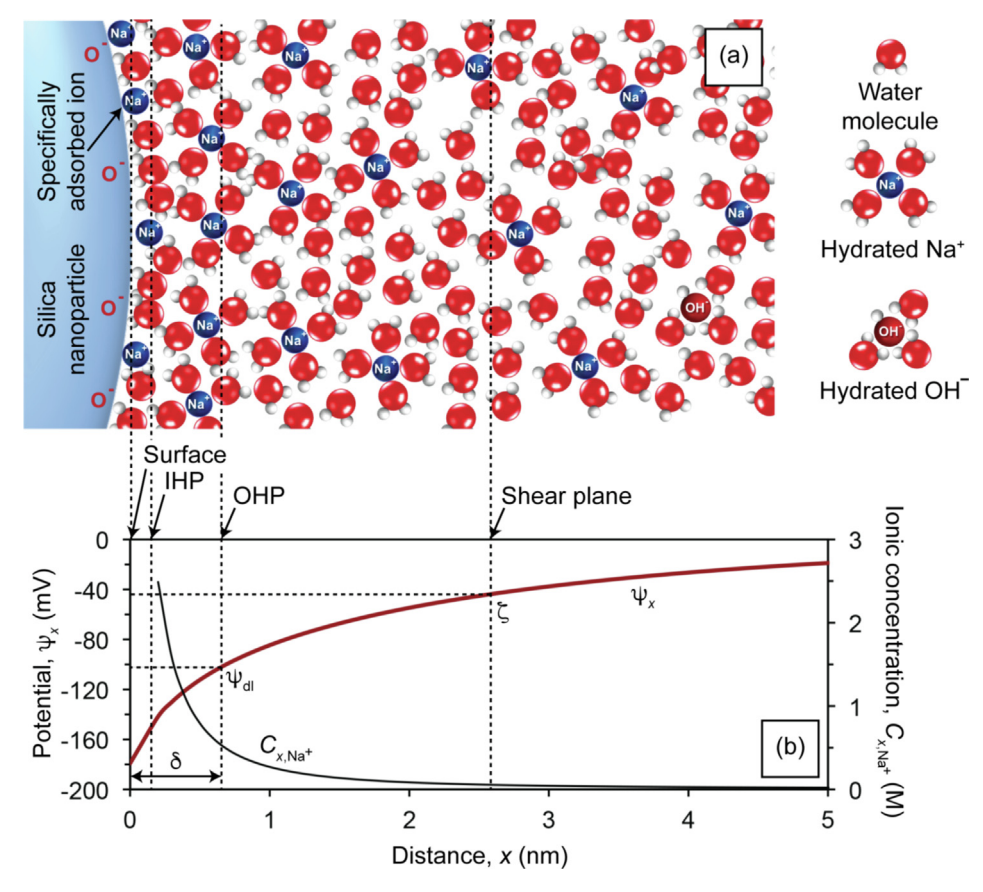


Fig. 4. (a) An illustration of the electrical double layer structure of a silanol-terminated silica nanoparticle aqueous solution at pH 12 based on (b) a potential profile and a dominant counterion (sodium cation) concentration distribution as a function of distance from the surface of the silica nanoparticles.

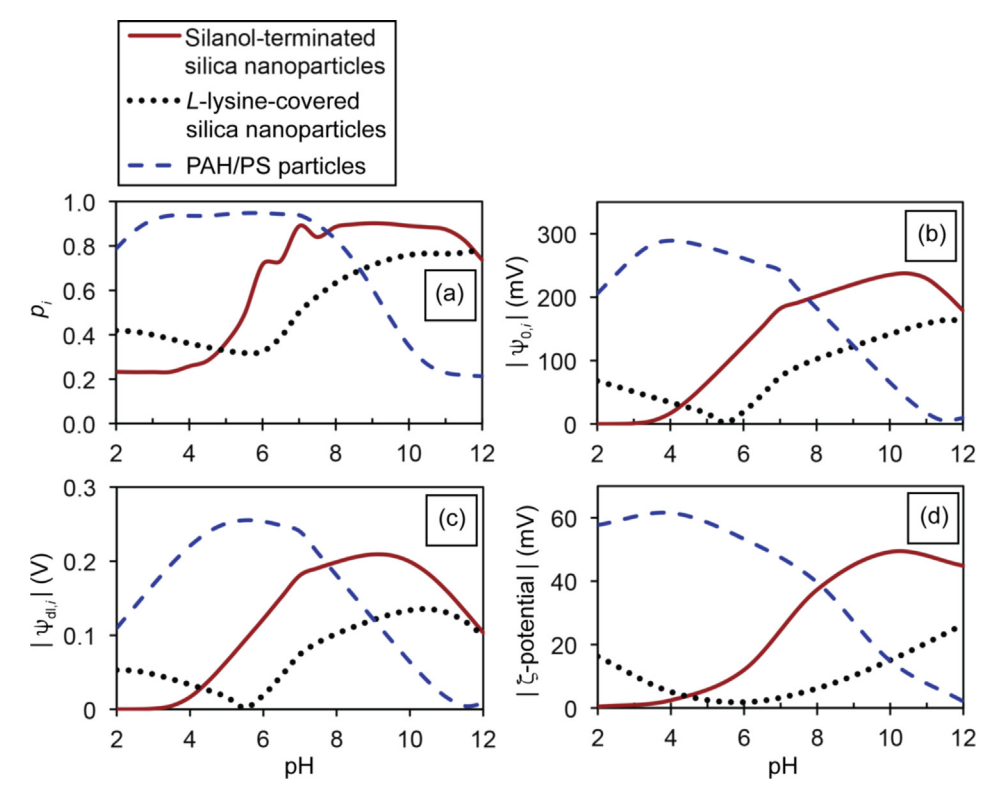


Fig. 5. (a) Regulation parameter, (b) absolute surface potential, (c) absolute diffuse layer potential, and (d) absolute ζ-potential profiles (based on measurements) for the silanol-terminated silica nanoparticles, ι-lysine-covered silica nanoparticles, and PAH/PS particles with respect to changes in pH.

sity of 0 [see Fig. 1(a)]. In the pH range from 4 to 7 where both surface charge density and ionic strength are weak, p_i drastically increases with an increase in pH and reaches a value of 0.86 at pH 7. From pH 7 to 11, both surface charge density and surface potential become stronger with constant p_i of 0.86. This shows that the surface charge density changes minimally for the particles upon approach in this pH range. Above pH 11, p_i decreases and reaches 0.74 at pH 12. This reduction in the value of p_i indicates that the surface charge density becomes more sensitive to the redistributed charges when the two silanol-terminated silica nanoparticles come closer.

The regulation parameter behavior of the ι -lysine silica nanoparticles is divided into three pH ranges, 2 to 6, 6 to 10, and 10 to 12. These pH ranges differ from those designated (pH 2 to 5, 5 to 7, and 7 to 12) in Fig. 2(c). This difference is discussed later. At pH values from 2 to 6, p_i decreases as the surface charge density decreases from a positive value to zero [see Fig. 1(a)]. At pH values from 6 to 10, p_i increases as the negative surface charge density becomes stronger. Above pH 10, p_i stays constant at a value of 0.75.

The slope of the regulation parameter of PAH/PS particles varies at four different pH ranges, 2 to 3, 3 to 7, 7 to 11, and 11 to 12. In the pH range of 2 and 3 where the high surface charge density value is constant at high ionic strength, p_i increases from 0.8 to 0.92. In this range, the strong surface charge density is constant for the approaching particles. In the pH range from 3 to 7, the constant p_i indicates that the surface charge density of the PAH/PS particles changes minimally when the separation distance approaches zero. There is a significant drop of the p_i value from pH 7 to 11 as the surface charge density becomes nearly zero [see Fig. 1(a)]. From pH 11 to 12, the constant p_i at 0.2 and the nearly zero surface charge density indicate that the surface potential undergoes small changes and the surface charge density is constant near zero for the approaching PAH/PS particles.

In order to justify that the computed p_i values generalize the EDL interaction energy and force for both symmetric and asymmetric colloidal systems, the regulation parameters for all the symmetric cases must be governed by the nonlinear relation between the surface charge density and the surface potential. The pH range of each regulation parameter of the silanol-terminated silica nanoparticles and the PAH/PS particles is divided the same as the pH ranges we defined for the surface charge density [Fig. 1(a)], the surface potential [Fig. 1(c)], and the ionic concentration on the surface [Fig. 2(b) and (d)]. However, the pH ranges for the regulation parameter of the L-lysine-covered silica nanoparticles are 2 to 6, 7 to 10 and 10 to 12, which are different from the pH ranges of 2 to 5, 5 to 7 and 7 to 12 of the surface charge density [Fig. 1(a)], the surface potential [Fig. 1(c)], and the ionic concentration on the surface [Fig. 2(c)]. With a premise that the regulation parameter cannot be negative, the trends of the regulation parameter behaviors [Fig. 5(a)] are similar to the absolute values of the computed surface potential profiles [Fig. 5(b)], the absolute values of the calculated diffuse layer potential [Fig. 5(c)], and the absolute values of empirically measured zeta potentials [Fig. 5(d)] for the surfaces of the silanol-terminated silica nanoparticles, the ι lysine-covered silica nanoparticles, and the PAH/PS particles. This is solid evidence to theoretically and experimentally support the validation of this regulation parameter. The absolute surface potential profiles in Fig. 5(b) are determined by taking absolute values of the surface potential data from Fig. 1(c). The absolute potential diagrams in Fig. 5(c) are calculated by taking absolute values of the computed potential [Equation (8)] at the outer Helmholtz plane determined in Table 1. Taking absolute values of the experimentally measured ζ-potential values in Fig. 3 gives the absolute ζ-potential distributions in Fig. 5(d).

From this analysis, we can conclude the following three general assessments. First, for the particles consisting of a single type of

ionizable functional group on the surface, the trend of the regulation parameter with variation of pH follows both the absolute values of the theoretically computed surface potentials and those of empirically measured ζ-potentials. Thus, without regulation parameter information, the charge regulation behavior of the particles upon approach is roughly expected from either surface potential or ζ-potential values. Second, the comparisons of surface charge density [Fig. 1(a)], ionic concentration on the surface [Fig. 2 (b), (c), and (d)], and regulation parameters [Fig. 5(a)], reveals the following correlations. As ionic strength increases, p_i decreases. As surface charge density increases, p_i increases. When both ionic strength and surface charge density increase, p_i is constant regardless of change in pH. Third, from the case of ι -lysine, which has an amphoteric surface having two different charges, we can flexibly design the surface of particles, which is characterized by a specific charge regulation behavior. This can be achieved by a combination of two or more different types of functional groups on the surface of the particles.

4.3. Pairwise DLVO interaction forces

Fig. 6(a)-(f) illustrate SEM images of the morphology of the deposited silanol-terminated silica nanoparticles on the PAH/PS particles with respect to pH. The morphology of these inorganicorganic composite particles is characterized by coverage of the silanol-terminated silica nanoparticles on PAH/PS particles and the presence of homoaggregation (aggregation with the same types of colloids) of the silanol-terminated silica nanoparticles. As seen in Fig. 6(a)-(f), the degree of coverage increases from the extreme pH (2 and 12) to neutral pH, and the homoaggregation of the silanol-terminated silica nanoparticles is observed at pH 2 and 4. The combination of these two phenomena determines their morphologies, namely homoaggregated silanol-terminated silica nanoparticles at pH 2 and 4, homoagglomerated (agglomeration with the same types of colloids) silanol-terminated silica nanoparticles at pH 6, densely-packed silanol-terminated silica nanoparticles at pH 8, and isolated silanol-terminated silica nanoparticles with small coverage at pH 10 and 12. Thus, to describe these two phenomena, namely the coverage and homoaggregation, we scrutinize the two different pairwise interactions: (i) an interaction between a silanol-terminated silica nanoparticle and a PAH/PS particle as depicted in the inset of Fig. 6(g) and (ii) an interaction between two silanol-terminated silica nanoparticles as illustrated in the inset of Fig. 6(j).

The degree of coverage is directly related to the heteroaggregation (aggregation with more than two different types of colloids) between silanol-terminated silica nanoparticles and PAH/PS particles. Thus, we investigate the pairwise DLVO interaction between these asymmetric particles to explain this phenomenon. Fig. 6(g) shows the vdW interaction force profile [Equation (SE1) in Supplementary Information], Fig. 6(h) presents the EDL interaction force profiles [Equation (11)] based on the regulation parameter we obtained earlier, and Fig. 6(i) displays the DLVO interaction force [Equation (1)] profiles. As seen in Fig. 6(g), the vdW force is constant regardless of the pH and the ionic strength of solution. Its attraction force becomes stronger at separation distances smaller than 0.5 nm, while it is very weak when that separation distance is greater. As plotted in Fig. 6(h), the EDL interaction force between the silanol-terminated silica nanoparticle and the PAH/PS particle is attractive in the entire pH range because of their oppositely charged surfaces. Overall, the magnitude of the pairwise EDL attractive force between the asymmetric surfaces is the strongest at pH 6 and 8, medium at pH 4 and 10, and weakest at pH 2 and 12. For pH values between 6 and 8, these strongest attraction forces originate from the higher surface potentials of both silanol-terminated silica nanoparticles and PAH/PS, as shown in

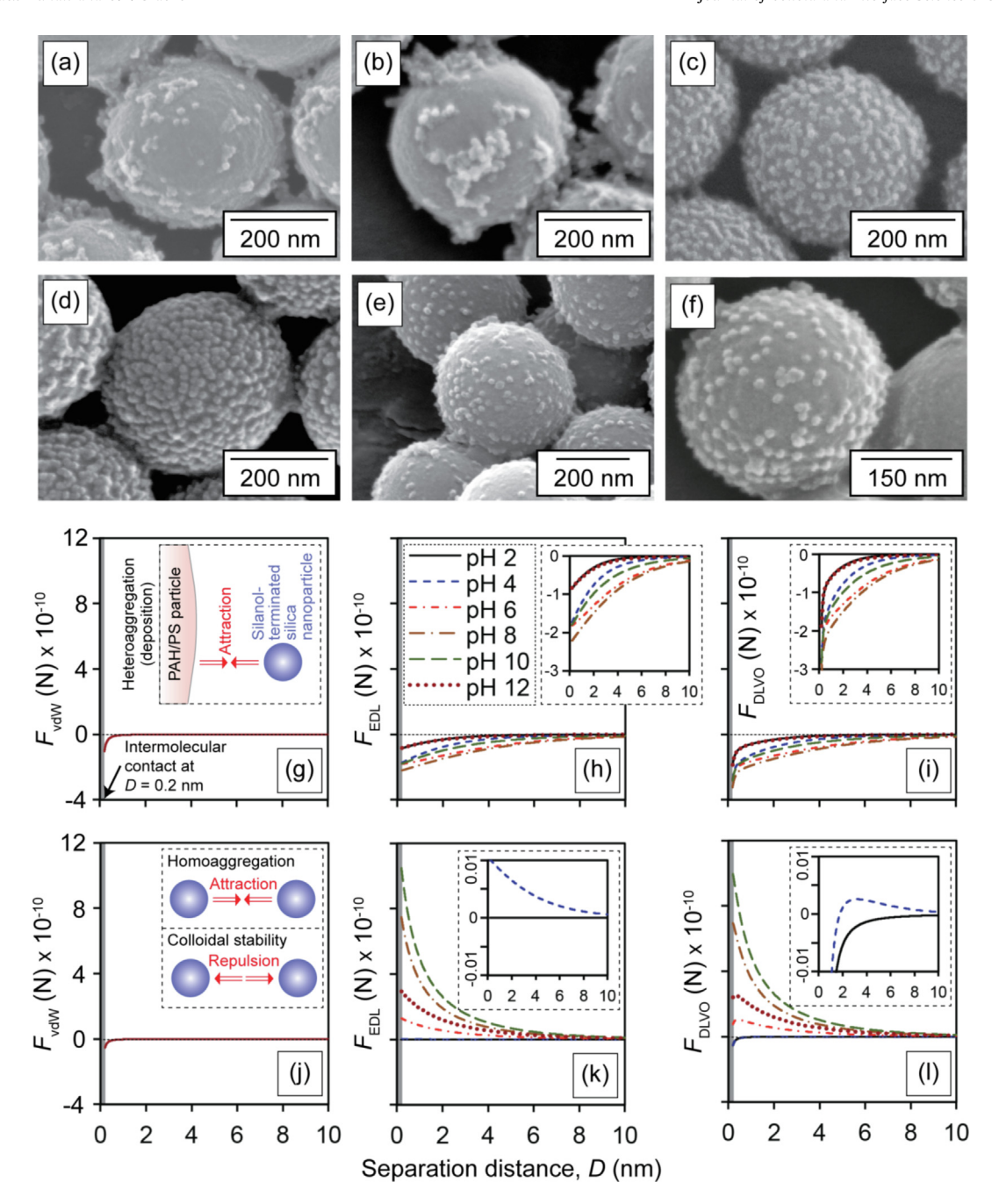


Fig. 6. Scanning electron micrographs of silanol-terminated silica nanoparticles deposited on PAH/PS particles prepared at (a) pH 2, (b) pH 4, (c) pH 6, (d) pH 8, (e) pH 10, and (f) pH 12. (g) Pairwise vdW interaction force profile, (h) pairwise EDL interaction force profile, and (i) pairwise DLVO interaction force profile for a silanol-terminated silica nanoparticle and a PAH/PS particle as a function of the separation distance with respect to pH. (j) Pairwise vdW interaction force profile, (k) pairwise EDL interaction force profile, and (l) pairwise DLVO interaction force profile for two silanol-terminated silica nanoparticles as a function of the separation distance with respect to pH.

Fig. 1(c). The next strong attraction forces at pH 4 and 10 are primarily determined by the weakest value of the regulation parameter of the silanol-terminated silica nanoparticle or the PAH/PS particle. For example, at pH 4 the regulation parameter of the silanol-terminated silica nanoparticles is 0.25 while that of the PAH/PS particles is 0.92. Moreover, at pH 10 the regulation parameter of the silanol-terminated silica nanoparticles is 0.88, but that of PAH/PS is 0.38. Likewise, the weakest attractive EDL forces seen at pH 2 and 12 are determined by the small regulation parameter value of the silanol-terminated silica nanoparticles at pH 2 ($p_i = 0.24$) and that of the PAH/PS particle at pH 12 ($p_i = 0.2$). From this analysis, we conclude that a surface having a smaller value of regulation parameter mainly limits the magnitude of the EDL inter-

action force. Fig. 6(i) displays the DLVO interaction forces for these asymmetric surfaces. If one compares Fig. 6(g), (h), and (i), the EDL attraction forces are dominant along the separation distance, while the relatively weak vdW force is only meaningful at the separation distance less than 0.5 nm. Thus, the EDL attraction force dominantly triggers an approach between the silanol-terminated silica nanoparticle and the PAH/PS particle. Once they are in intermolecular contact at D=0.2 nm, this EDL interaction force mainly holds these two particles together. In addition, the vdW force contributes to holding the silanol-terminated silica nanoparticle on the PAH/PS particle more tightly. If we take a closer look at both Fig. 6(a)-(f) and 6(i), the coverage trend of the silanol-terminated silica nanoparticles on the PAH/PS particle matches well as pH is varied.

The degree of nanoparticle coverage is proportional to the magnitude of the attractive DLVO force. The strongest DLVO force profiles at pH 6 and 8 agree with the highest coverage of the silanol-terminated silica nanoparticles on the PAH/PS particle. The medium strength of the DLVO forces at pH 4 and 10 is correlated to the medium coverage of the nanoparticles. The weakest DLVO forces at pH 2 and 12 correspond with the lowest coverage of the silica nanoparticles. Thus, to increase the coverage of these silanol-terminated silica nanoparticles on the PAH/PS particles, we can increase the value of the regulation parameter.

The second factor that affects the morphology of these inorganic/organic nanocomposite particles is homoaggregation of the silanol-terminated silica nanoparticles. As illustrated in the inset of Fig. 6(j), these particles undergo homoaggregation under attractive forces, while exhibiting good colloidal stability under repulsive force. This trend can be explained by the DLVO interaction force profiles for the two symmetric silanol-terminated silica nanoparticles. Fig. 6(j) represents the vdW interaction force [Equation (SE1) in Supplementary Information], Fig. 6(k) displays the EDL interaction force [Equation (11)], and Fig. 6(1) shows the DLVO interaction force [Equation (1)] profiles. As seen in Fig. 6(j), at intermolecular contact, the vdW force between the two silanol-terminated silica nanoparticles is also constant regardless of pH and ionic strength of the solution. Its magnitude is almost half of the vdW force between the silanol-terminated silica nanoparticles and the PAH/ PS particle, compared with Fig. 6(g) and (j). This attractive vdW force is only valid when the separation distance is less than 0.3 nm. This is mainly because higher numbers of atoms can be instantaneously polarized in the large PAH/PS particle and can exert London dispersion forces between the small nanoparticle and the large PAH/PS particle. Fig. 6(k) shows that the EDL force for these symmetric surfaces increases in order from pH 2, 4, 6, 12, 8, and 10. This tendency agrees with the regulation parameter profile for the silanol-terminated silica nanoparticles as displayed in Fig. 5(a). As discussed earlier, the surface charge density of the silanol-terminated silica nanoparticles increases as pH increases. The regulation parameter considers that the surface potential drops with respect to the ionic strength of the solution so that the surface at pH 12 shows attenuated repulsive force. As displayed in Fig. 6(1), the overall DLVO interaction force profiles for this symmetric system with respect to pH are dominantly governed by the EDL interaction force profiles. In this case, the physically meaningful role of the vdW force is to offset the very weak repulsive EDL force at pH 2 and 4 and change it to an attractive force as confirmed in Fig. 6(1). This result supports the homoaggregation of the silanol-terminated silica nanoparticles seen in the SEM images for pH 2 and 4 in Fig. 6(a)-(f). If we look at the SEM image for pH 6, most silanol-terminated silica nanoparticles are partially in contact with each other although the DLVO profile for this pH shows repulsive force. This is because when more nanoparticles are attached to the other surface, the redistribution of ionic species occurs, resulting in changes of both surface charge density and surface potential. Thus, the actual strength of this repulsive force between the silica nanoparticles, which are attached on the PAH/PS particle, should be attenuated from the computed DLVO force. The total repulsive force at intermolecular contact for pH 6 is not strong enough to isolate all the attached silanol-terminated silica nanoparticles on the PAH/PS particle. The other DLVO profiles at pH 8, 10, and 12 show strong repulsive forces so that all the attached silanol-terminated silica nanoparticles on the PAH/PS particles are likely to be isolated as confirmed in the SEM images for pH 8, 10, and 12 in Fig. 6(a)-(f).

Fig. 7(a)-(f) illustrate a series of SEM images illustrating the changes in the morphology of the deposited ι -lysine-covered silica nanoparticles on the PAH/PS particle with respect to pH. As discussed earlier, the change in these morphologies can be explained by both the degree of the ι -lysine-covered silica nanoparticle cov-

erage on PAH/PS and the homoaggregation of the L-lysine-covered silica nanoparticles. As seen in Fig. 7(a)-(b), the deposition of the L-lysine-covered silica nanoparticles does not occur at pH 2 and 4. According to the SEM images, the degree of coverage increases in order of 12, 6, 10, and 8. Weak homoaggregation of the Llysine-covered silica nanoparticles creates clustering at pH 6 [Fig. 7(c)] and bridging at pH 8 [Fig. 7(d)]. These changes in morphology with pH are summarized in Table 2. We find that there is no L-lysine-covered silica nanoparticle deposition at pH 2 and 4, clustered L-lysine-covered silica nanoparticles at pH 6, densely-packed L-lysine-covered silica nanoparticles with slight homoagglomeration at pH 8, and isolated nanoparticles with smaller coverage at pH 10 and 12. In order to explain this change in morphology, we explore the two different pairwise interactions: (i) an interaction between an *L*-lysine-covered silica nanoparticle and a PAH/PS particle as depicted in the inset of Fig. 7(g) and (ii) an interaction between two L-lysine-covered silica nanoparticles as illustrated in the inset of Fig. 7(j).

The degree of coverage of the L-lysine-covered silica nanoparticles on PAH/PS is described by the pairwise DLVO interaction force of these asymmetric particles. Fig. 7(g) displays the vdW interaction force [Equation (SE1) in Supplementary Information], Fig. 7 (h) represents the EDL interaction force [Equation (11)] based on the regulation parameter, and Fig. 7(i) plots the DLVO interaction force [Equation (1)] profile. As seen in Fig. 7(g), the attractive vdW force starts drastically increasing at D = 1 nm, and its magnitude at intermolecular contact is two times higher than the vdW force between the silanol-terminated silica nanoparticle and the PAH/PS particle [see Fig. 6(g)]. The large difference in these vdW forces originates from the fact that more atoms of the ι -lysine layer undergo instantaneous dipole-induced dipole forces than those of silica. Because the amphoteric surface of the L-lysine can have positive, neutral, and negative charge depending on pH [see Fig. 1(a)], the EDL interaction force profiles between the L-lysine-covered silica nanoparticles and PAH/PS particle at pH 2 and 4 are attractive, and those at pH 6, 8, 10, and 12 are repulsive as plotted in Fig. 7(h). If we take a closer look at the most interesting EDL interaction force profile at pH 4, this weak repulsive force becomes weaker as the separation distance approaches zero. This indicates that our nonlinear charge regulation model describes the attenuation of the surface charge density, which is caused by the redistribution of ionic species when these two asymmetric particles are approaching. For the attractive EDL interaction forces, their strength increases in order of pH 12, 6, 10, and 8. As seen in Fig. 7(i), the DLVO interaction force profiles for separation distances larger than 0.5 nm are dominantly governed by the EDL interaction forces, whereas those at a separation distance less than 0.5 nm are mostly governed by the strong vdW forces. The repulsive DLVO forces at pH 2 and 4 agree with a lack of deposition of the L-lysine-covered silica nanoparticles on the PAH/PS particle, as seen in Fig. 6(a)-(b). Because the vdW force is constant regardless of pH of the solution, the tendency of the strength of the DLVO interaction force depends on the EDL interaction force, and the magnitude of the attractive DLVO force also increases in order of pH 12, 6, 10, and 8. This trend of the attraction force profiles show good agreements with the degree of coverage of the 1-lysinecovered silica nanoparticles on the PAH/PS particles as confirmed in the SEM images for pH 6, 8, 10, and 12 of Fig. 7(c)-(f).

The homoaggregation of the ι -lysine-covered silica nanoparticles occurs when there is attraction between these as illustrated in the inset of Fig. 7(j). In contrast, when there is a strong repulsion between them, they show good colloidal stability. Fig. 7(j) presents the vdW interaction force [Equation (SE1) in Supplementary Information], Fig. 7(k) shows the EDL interaction force [Equation (11)], and Fig. 7(l) shows the DLVO interaction force [Equation (1)] pro-

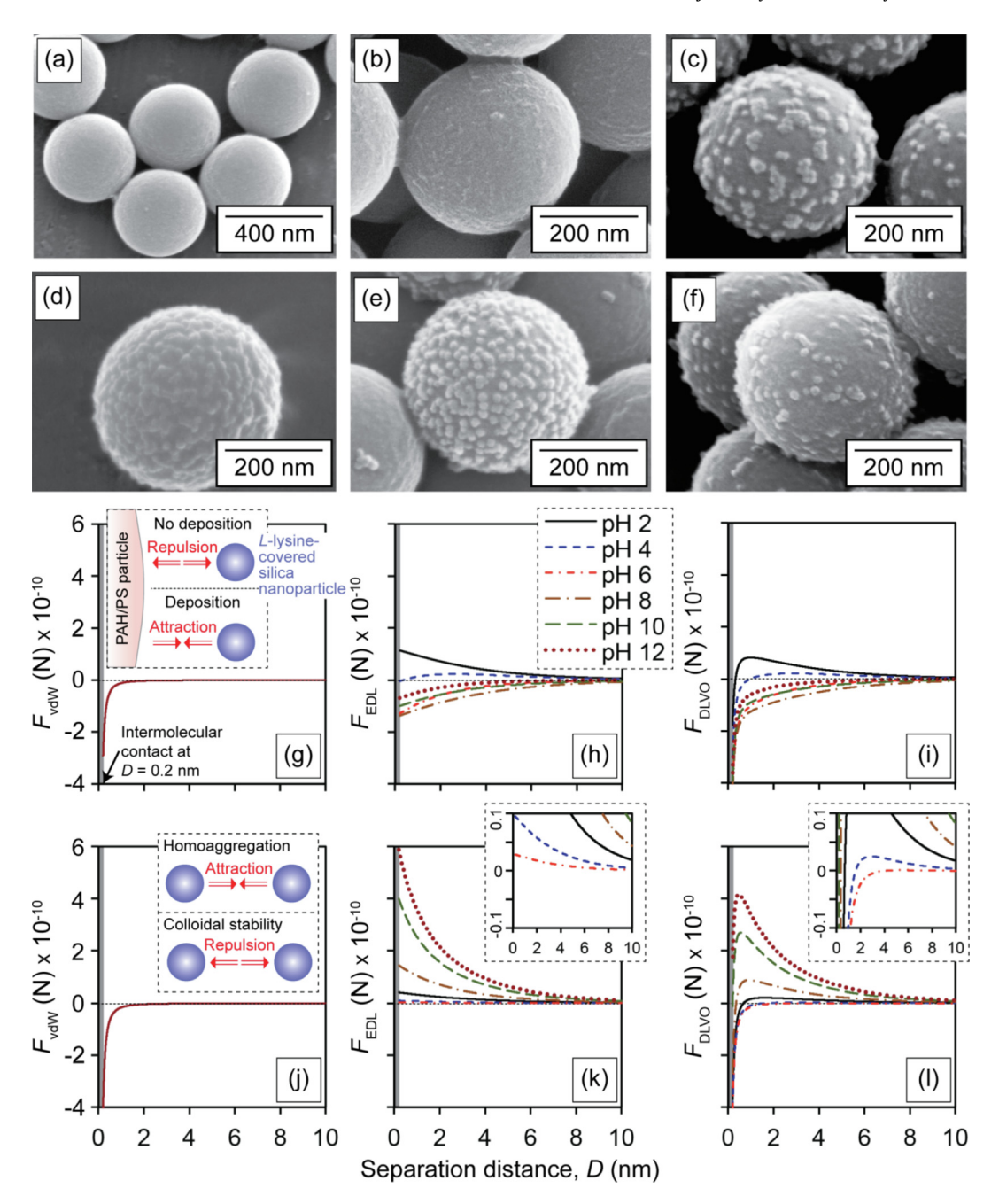


Fig. 7. Scanning electron micrographs of *ι*-lysine-covered silica nanoparticles deposited on PAH/PS particles prepared at (a) pH 2, (b) pH 4, (c) pH 6, (d) pH 8, (e) pH 10, and (f) pH 12. (g) Pairwise vdW interaction force profile, (h) pairwise EDL interaction force profile, and (i) pairwise DLVO interaction force profile for an *ι*-lysine-covered silica nanoparticle and a PAH/PS particle as a function of the separation distance with respect to pH. (j) Pairwise vdW interaction force profile, (k) pairwise EDL interaction force profile, and (l) pairwise DLVO interaction force profile for two *ι*-lysine-covered silica nanoparticles as a function of the separation distance with respect to pH.

Table 2Summary of deposition behavior of silanol-terminated silica nanoparticles on PAH/PS and ι -lysine-covered silica nanoparticles on PAH/PS with respect to pH of solutions.

рН	(1) Silanol-terminated silica Silanol-terminated silica nano-particles ^(a)	nanoparticles on PAH/PS Silanol-terminated silica nano- particles and PAH/PS ^(b)	Coverage	(2) <i>L</i> -lysine-covered silica <i>L</i> -lysine-covered silica nano-particles (a)	nanoparticles on PAH/PS <i>L</i> -lysine-covered silica nano- particles and PAH/PS ^(b)	Coverage
2	Homo-aggregation	Hetero-aggregation	Low	Repulsion	Repulsion	None
4	Homo-aggregation		Low	Homo-aggregation	Repulsion	None
6	Homo-agglomeration		High	Homo-aggregation	Hetero-aggregation	Medium
8	Isolated		High	Homo-agglomeration	Hetero-aggregation	High
10	Isolated		Medium	Isolated	Hetero-aggregation	High
12	Isolated		Medium	Isolated	Hetero-aggregation	Low

 $^{^{(}a)}$ Colloidal stability behavior between small silica nanoparticles.

⁽b) Colloidal stability behavior between a large PAH/PS particle and small silica nanoparticles.

files. As seen in Fig. 7(j), the attractive vdW force starts rising at D = 1.1 nm, and its magnitude at intermolecular contact (D = 0.2 nm) is seven times higher than the vdW force between the silanol-terminated silica nanoparticles [see Fig. 6(j)]. As explained earlier, this difference is due to the high density of atoms of the ι -lysine layer. The EDL repulsive force plotted in Fig. 7(k) increases in order of pH 6, 4, 2, 8, 10, and 12. This trend for the symmetric *L*-lysine-covered silica nanoparticles matches the corresponding regulation parameter as plotted in Fig. 5(a). Although the EDL interaction force seems dominant across all separation distance ranges by comparing Fig. 7(k) and 7(l), the degree of contribution of each vdW and EDL interaction force to the DLVO interaction force profile is different depending on the pH of the solution and the separation distance. For pH 4 and 6, the vdW forces start effectively affecting these two symmetric surfaces at a separation distance of 2.8 nm and 5 nm, respectively, where the derivatives of the DLVO forces with respect to the separation distance are zero. For pH 2, 8, 10, and 12, these symmetric particles are primarily governed by the vdW force at a separation distance less than 0.5 nm. For the samples having deposited *L*-lysine silica nanoparticles, the DLVO interaction force increases in order of 6, 8, 10, and 12. The DLVO force profile at pH 6 shows attractive force and agrees with the clustered *L*-lysine-covered silica nanoparticles on the PAH/PS particle in the SEM images of Fig. 7(a)-(f). Although the DLVO profile for pH 8 shows weak repulsive force, its value is not enough to prevent the homoaggregation of the L-lysinecovered silica nanoparticles when many of them are attached on the PAH/PS particle, forming dense packing and connections between them on the PAH/PS particle. As discussed earlier, this is because the substrate particle with attached small particles, loses surface charge density during redistribution of ions. Both DLVO force profiles of pH 10 and 12 [Fig. 7(1)] show strong repulsion so that the deposited L-lysine-covered silica nanoparticles are isolated on the PAH/PS particle.

In summary, our modified EDL model is based on a regulation parameter that describes realistic charge regulation. The pairwise DLVO interaction force profile, based on this modified EDL model. effectively describes both symmetric and asymmetric particles. Since this regulation parameter describes realistic charge regulation phenomena depending on pH, total salt concentration, ionic strength, and separation distance, our EDL model is extended to mathematically explain practical situations such as low and high ionic strength and low and high surface potential cases. This single DLVO model can describe both the heteroaggregation between a silica nanoparticle and a PAH/PS particle and homoaggregation between two identical silica nanoparticles. This analysis explains the deposition behavior of silanol-terminated silica nanoparticles and ι-lysine-covered silica nanoparticles on amine-functionalized PAH/PS particles with respect to pH. In addition, we also see the possibility for flexibly designing the particle surface to control charge regulation behavior, which can be achieved by combinations of multi-functional groups on the particle surfaces. Thus, we propose that this regulation parameter model, under the nonlinear charge regulation relation and the ionic size-determined diffuse layer potential, generalizes pairwise EDL interaction force and energy for both symmetric and asymmetric surfaces and extends its applications for low to high ionic strength and low to high surface potential cases.

5. Conclusions

In this study, we introduced an experimental method and a modified DLVO model to elucidate and predict mechanisms that can finely control the morphologies of inorganic nanoparticles physically deposited on the surface of submicron-sized organic

particles in a water solution. To compare the results of the experiments with the theoretical values from our model, we prepared silanol-terminated silica nanoparticles and amphoteric L-lysinecovered silica nanoparticles. Also, PAH monolayer-coated polystyrene sub-micrometer particles were prepared as a substrate. The two different types of silica nanoparticles were physisorbed onto the PAH/PS particles at different pH conditions, and morphologies were analyzed by scanning electron microscopy. To theoretically characterize the difference in the deposition behaviors of these two types of silica particles to PAH/PS particles, we describe heteroaggregation between a silica particle and a polystyrene particle and homoaggregation between two identical silica particles. To illustrate these two phenomena mathematically, we used a modified DLVO model, which describes pairwise interactions for both symmetric and asymmetric surfaces. In the vdW interaction force term, the surface roughness of the particles greatly influences the classical London dispersion force, thus verification of the surfaces of the synthesized particles was completed using scanning and transmission electron microscopy to minimize the error caused by significant roughness of the particle surfaces. To develop our EDL interaction model, the nonlinear charge regulation relation between surface charge density and surface potential was described by defining the acid-base reaction of the functional groups on the colloidal surface with respect to pH. Compared to previously reported regulation parameter models [21-22,26-28,32], we theoretically calculated a constant regulation parameter for each case based on the nonlinear charge regulation of surface charge density and surface potential. Then, the pairwise EDL interaction force was generalized by introducing the regulation parameter, which describes the realistic charge regulation phenomenon as a function of pH, total salt concentration, ionic strength of the solution, and the separation distance. We found that the trend of this regulation parameter can be roughly estimated by the absolute values of theoretically calculated surface potentials and diffuse layer potentials, as well as the absolute values of experimentally measured ζ-potentials. We expect that one can design the desired charge regulation behaviors of colloidal systems at specific pH values by placing more than two different types of functional groups on the colloidal particles. The sum of the vdW and the EDL interaction forces for both symmetric and asymmetric surfaces describes the pH-dependency of the deposition behaviors of inorganic nanoparticles on sub-micrometer organic substrate particles. Thus, we propose that the regulation parameter based on our nonlinear charge regulation model generalizes the EDL interaction term so that the DLVO model describes both symmetric and asymmetric surfaces, as well as low to high ionic strength and low to high potential cases. This model is expected to contribute to the design of organic/inorganic hybrid nanoparticles.

CRediT authorship contribution statement

Seongcheol Choi: Conceptualization, Data curation, Formal analysis, Investigation, Methodology, Visualization, Writing – original draft, Writing – review & editing. **Rafael Vazquez-Duhalt:** Conceptualization, Methodology, Resources, Validation, Writing – review & editing. **Olivia A. Graeve:** Conceptualization, Funding acquisition, Methodology, Project administration, Resources, Validation, Visualization, Writing – review & editing.

Declaration of Competing Interest

The authors declare that they have no known competing financial interests or personal relationships that could have appeared to influence the work reported in this paper.

Acknowledgements

This work was supported by a grant from the National Science Foundation (No. 1911372) and funding from the UC-Mexico Initiative of the University of California Office of the President.

Appendix A. Supplementary data

Supplementary data to this article can be found online at https://doi.org/10.1016/j.jcis.2022.01.076.

References

- [1] Z. Zhang, P. Zhang, Y. Wang, W. Zhang, Recent advances in organic-inorganic well-defined hybrid polymers using controlled living radical polymerization techniques, Polym. Chem. 7 (24) (2016) 3950–3976.
- [2] J. Lee, C.K. Hong, S. Choe, S.E. Shim, Synthesis of polystyrene/silica composite particles by soap-free emulsion polymerization using positively charged colloidal silica, J. Colloid Interface Sci. 310 (1) (2007) 112–120.
- [3] W.K. Tan, Y. Araki, A. Yokoi, G. Kawamura, A. Matsuda, H. Muto, Micro- and nano-assembly of composite particles by electrostatic adsorption, Nanoscale Res. Lett. 14 (2019) 297–305.
- [4] M. Hood, M. Mari, R. Muñoz-Espí, Synthetic strategies in the preparation of polymer/inorganic hybrid nanoparticles, Materials 7 (5) (2014) 4057–4087.
- [5] F. Caruso, H. Lichtenfeld, M. Giersig, H. Möhwald, Electrostatic self-assembly of silica nanoparticle-polyelectrolyte multilayers on polystyrene latex particles, J. Am. Chem. Soc. 120 (33) (1998) 8523–8524.
- [6] P.B. Landon, A.H. Mo, C. Zhang, C.D. Emerson, A.D. Printz, A.F. Gomez, C.J. DeLaTorre, D.A.M. Colburn, P. Anzenberg, M. Eliceiri, C. O'Connell, R. Lal, Designing hollow nano gold golf balls, ACS Appl. Mater. Interfaces 6 (13) (2014) 9937–9941.
- [7] H. Satoh, H. Yabu, One-pot preparation of organic-inorganic composite microspheres comprising silica nanoparticles and end-functionalized polymers, Macromol. Mater. Eng. 301 (3) (2016) 279–286.
- [8] A. Suhendi, A.B.D. Nandiyanto, T. Ogi, K. Okuyama, Agglomeration-free coreshell polystyrene/silica particles preparation using an electrospray method and additive-free cationic polystyrene core, Mater. Lett. 91 (2013) 161–164.
- [9] V. Fischer, M.B. Bannwarth, G. Jakob, K. Landfester, R. Muñoz-Espí, Luminescent and magnetoresponsive multifunctional chalcogenide/polymer hybrid nanoparticles, J. Phys. Chem. C 117 (11) (2013) 5999–6005.
- [10] Y. Lu, Y. Mei, M. Drechsler, M. Ballauff, Thermosensitive core-shell particles as carriers for Ag nanoparticles: modulating the catalytic activity by a phase transition in networks, Angew. Chem. Int. Ed. 45 (5) (2006) 813–816.
- [11] C. Tian, B. Mao, E. Wang, Z. Kang, Y. Song, C. Wang, S. Li, Simple strategy for preparation of core colloids modified with metal nanoparticles, J. Phys. Chem. C 111 (9) (2007) 3651–3657.
- [12] M. Schrinner, M. Ballauff, Y. Talmon, Y. Kauffmann, J. Thun, M. Moller, J. Breu, Single nanocrystals of platinum prepared by partial dissolution of Au-Pt nanoalloys, Science 323 (5914) (2009) 617–620.
- [13] V. Fischer, I. Lieberwirth, G. Jakob, K. Landfester, R. Muñoz-Espí, Metal oxide/ polymer hybrid nanoparticles with versatile functionality prepared by controlled surface crystallization, Adv. Funct. Mater. 23 (4) (2013) 451–466.
- [14] Z. Yang, Z. Niu, Y. Lu, Z. Hu, C.C. Han, Templated synthesis of inorganic hollow spheres with a tunable cavity size onto core-shell gel particles, Angew. Chem. Int. Ed. 42 (17) (2003) 1943–1945.
- [15] Z. Xu, A. Xia, C. Wang, W. Yang, S. Fu, Synthesis of raspberry-like magnetic polystyrene microspheres, Mater. Chem. Phys. 103 (2–3) (2007) 494–499.
- [16] M. Feyen, C. Weidenthaler, F. Schüth, A.-H. Lu, Regioselectively controlled synthesis of colloidal mushroom nanostructures and their hollow derivatives, J. Am. Chem. Soc. 132 (19) (2010) 6791–6799.
- [17] N. Negrete-Herrera, J.-L. Putaux, L. David, F.D. Haas, E. Bourgeat-Lami, Polymer/Laponite composite latexes: particle morphology, film microstructure, and properties, Macromol. Rapid Commun. 28 (15) (2007) 1567–1573.
- [18] S. Reculusa, C. Mingotaud, E. Bourgeat-Lami, E. Duguet, S. Ravaine, Synthesis of daisy-shaped and multipod-like silica/polystyrene nanocomposites, Nano Lett. 4 (9) (2004) 1677–1682.
- [19] Y. Fukui, K. Fujimoto, Bio-inspired nanoreactor based on a miniemulsion system to create organic-inorganic hybrid nanoparticles and nanofilms, J. Mater. Chem. A 22 (8) (2012) 3493–3499.
- [20] A. Hamberger, U. Ziener, K. Landfester, Encapsulation of in situ nanoprecipitated inorganic materials in confined geometries into a polymer shell using inverse miniemulsion, Macromol. Chem. Phys. 214 (6) (2013) 691– 699.
- [21] G. Trefalt, I. Szilagyi, M. Borkovec, Poisson-Boltzmann description of interaction forces and aggregation rates involving charged colloidal particles in asymmetric electrolytes, J. Colloid Interface Sci. 406 (2013) 111–120.
- [22] G. Trefalt, F.J.M. Ruiz-Cabello, M. Borkovec, Interaction forces, heteroaggregation, and deposition involving charged colloidal particles, J. Phys. Chem. B 118 (23) (2014) 6346–6355.
- [23] M. Elzbieciak-Wodka, M.N. Popescu, F.J.M. Ruiz-Cabello, G. Trefalt, P. Maroni, M. Borkovec, Measurements of dispersion forces between colloidal latex

- particles with the atomic force microscope and comparison with Lifshitz theory, J. Chem. Phys. 140 (2014) 104906.
- [24] B.W. Ninham, On progress in forces since the DLVO theory, Adv. Colloid Interface Sci. 83 (1-3) (1999) 1–17.
- [25] J.N. Israelachvili, Intermolecular and Surface Forces, 3rd ed., Academic Press, 2011
- [26] S.H. Behrens, M. Borkovec, Electrostatic interaction of colloidal surfaces with variable charge, J. Phys. Chem. B 103 (15) (1999) 2918–2928.
- [27] I. Popa, P. Sinha, M. Finessi, P. Maroni, G. Papastavrou, M. Borkovec, Importance of charge regulation in attractive double-layer forces between dissimilar surfaces, Phys. Rev. Lett. 104 (22) (2010) 228301.
- [28] F.J. Montes Ruiz-Cabello, G. Trefalt, P. Maroni, M. Borkovec, Electric double-layer potentials and surface regulation properties measured by colloidal-probe atomic force microscopy, Phys. Rev. E 90 (1) (2014) 012301.
- [29] A.M. Smith, P. Maroni, M. Borkovec, G. Trefalt, Measuring inner layer capacitance with the colloidal probe technique, Colloids Interfaces 2 (4) (2018) 65.
- [30] A.M. Smith, M. Borkovec, G. Trefalt, Forces between solid surfaces in aqueous electrolyte solutions, Adv. Colloid Interface Sci. 275 (2020) 102078.
- [31] B. Uzelac, V. Valmacco, G. Trefalt, Interactions between silica particles in the presence of multivalent coions, Soft Matter 13 (34) (2017) 5741–5748.
- [32] S.H. Behrens, M. Borkovec, Exact Poisson-Boltzmann solution for the interaction of dissimilar charge-regulating surfaces, Phys. Rev. E 60 (6) (1999) 7040–7048.
- [33] S.L. Carnie, D.Y.C. Chan, interaction free energy between plates with charge regulation: A linearized model, J. Colloid Interface Sci. 161 (1) (1993) 260–264.
- [34] J. Wang, A. Sugawara-Narutaki, M. Fukao, T. Yokoi, A. Shimojima, T. Okubo, Two-phase synthesis of monodisperse silica nanospheres with amines or ammonia catalyst and their controlled self-assembly, ACS Appl. Mater. Interfaces 3 (5) (2011) 1538–1544.
- [35] B. Quan, C. Lee, J.S. Yoo, Y. Piao, Facile scalable synthesis of highly monodisperse small silica nanoparticles using alkaline buffer solution and their application for efficient sentinel lymph node mapping, J. Mater. Chem. B 5 (3) (2017) 586–594.
- [36] T. Yokoi, Y. Sakamoto, O. Terasaki, Y. Kubota, T. Okubo, T. Tatsumi, Periodic arrangement of silica nanospheres assisted by amino acids, J. Am. Chem. Soc. 128 (42) (2006) 13664–13665.
- [37] T.M. Davis, M.A. Snyder, J.E. Krohn, M. Tsapatsis, Nanoparticles in lysine-silica sols, Chem. Mater. 18 (25) (2006) 5814–5816.
- [38] T. Yokoi, M. Iwama, R. Watanabe, Y. Sakamoto, O. Terasaki, Y. Kubota, J.N. Kondo, T. Okubo, T. Tatsumi, Synthesis of well-ordered nanospheres with uniform mesopores assisted by basic amino acids, Stud. Surf. Sci. Catal. 170 (2007) 1774–1780.
- [39] K.D. Hartlen, A.P.T. Athanasopoulos, V. Kitaev, Facile preparation of highly monodisperse small silica spheres (15 to > 200 nm) suitable for colloidal templating and formation of ordered arrays, Langmuir 24 (2008) 1714–1720.
- [40] D. Breite, M. Went, A. Prager, A. Schulze, Tailoring membrane surface charges: A novel study on electrostatic interactions during membrane fouling, Polymers 7 (10) (2015) 2017–2030.
- [41] O.J. Rojas, M. Ernstsson, R.D. Neuman, P.M. Claesson, Effect of polyelectrolyte charge density on the adsorption and desorption behavior on mica, Langmuir 18 (5) (2002) 1604–1612.
- [42] H. Gong, J. Garcia-Turiel, K. Vasilev, O.I. Vinogradova, Interaction and adhesion properties of polyelectrolyte multilayers, Langmuir 21 (16) (2005) 7545-7550.
- [43] W.J. Dressick, K.J. Wahl, N.D. Bassim, R.M. Stroud, D.Y. Petrovykh, Divalentanion salt effects in polyelectrolyte multilayer depositions, Langmuir 28 (45) (2012) 15831–15843.
- [44] J. Hierrezuelo, A. Sadeghpour, I. Szilagyi, A. Vaccaro, M. Borkovec, Electrostatic stabilization of charged colloidal particles with adsorbed polyelectrolytes of opposite charge, Langmuir 26 (19) (2010) 15109–15111.
- [45] Z. Feldötö, I. Varga, E. Blomberg, E. Blomberg, Influence of salt and rinsing protocol on the structure of PAH/PSS polyelectrolyte multilayers, Langmuir 26 (22) (2010) 17048–17057.
- [46] R.E. Ridley, H. Fathi-Kelly, J.P. Kelly, V.R. Vasquez, O.A. Graeve, Predicting the size of salt-containing aqueous Na-AOT reverse micellar water-in-oil microemulsions with consideration for specific ion effects, J. Colloid Interface Sci. 586 (2021) 830–835.
- [47] R.E. Ridley, E. Alvarado, A.A. Mrse, V.R. Vasquez, O.A. Graeve, Phase stability and miscibility in ethanol/AOT/n-heptane systems: Evidence of multilayered cylindrical and spherical microemulsion morphologies, Langmuir 36 (38) (2020) 11274–11283.
- [48] J.T. Cahill, J.N. Ruppert, B. Wallis, Y. Liu, O.A. Graeve, Development of mesoporosity in scandia-stabilized zirconia: Particle size, solvent, and calcination effects, Langmuir 30 (19) (2014) 5585–5591.
- [49] C.I. Vargas-Consuelos, K. Seo, M. Camacho-López, O.A. Graeve, Correlation between particle size and raman vibrations in WO₃ powders, J. Phys. Chem. C 118 (18) (2014) 9531–9537.
- [50] O.A. Graeve, H. Fathi, J.P. Kelly, M.S. Saterlie, K. Sinha, G. Rojas-George, R. Kanakala, D.R. Brown, E.A. Lopez, Reverse micelle synthesis of oxide nanopowders: Mechanisms of precipitate formation and agglomeration effects, J. Colloid Interface Sci. 407 (2013) 302–309.
- [51] M.S. Saterlie, H. Sahin, B. Kavlicoglu, Y. Liu, O.A. Graeve, Surfactant effects on dispersion characteristics of copper-based nanofluids: A dynamic light scattering study, Chem. Mater. 24 (17) (2012) 3299–3306.
- [52] H. Fathi, J.P. Kelly, V.R. Vasquez, O.A. Graeve, Ionic concentration effects on reverse micelle size and stability: Implications for the synthesis of nanoparticles, Langmuir 28 (25) (2012) 9267–9274.

- [53] M. Saterlie, H. Sahin, B. Kavlicoglu, Y. Liu, O. Graeve, Particle size effects in the thermal conductivity enhancement of copper-based nanofluids, Nanoscale Res. Lett. 6 (1) (2011) 217.
- [54] V.R. Vasquez, B.C. Williams, O.A. Graeve, Stability and comparative analysis of AOT/water/isooctane reverse micelles system using dynamic light scattering and molecular dynamics, J. Phys. Chem. B 115 (12) (2011) 2979–2987.
- [55] K. Sinha, B. Pearson, S.R. Casolco, J.E. Garay, O.A. Graeve, Synthesis and consolidation of BaAl₂Si₂O₈:Eu: Development of an integrated process for luminescent smart ceramic materials, J. Am. Ceram. Soc. 92 (11) (2009) 2504–2511.
- [56] K. Sinha, B. Kavlicoglu, Y. Liu, F. Gordaninejad, O.A. Graeve, A comparative study of thermal behavior of iron and copper nanofluids, J. Appl. Phys. 106 (6) (2009) 064307.
- [57] O.A. Graeve, K. Sinha, Dynamic light scattering study of reverse micellar systems for the synthesis of iron-based nanofluids, Int. J. Mod. Phys. B 21 (28n29) (2007) 4774–4781.
- [58] M. Barisik, S. Atalay, A. Beskok, S. Qian, Size dependent surface charge properties of silica nanoparticles, J. Phys. Chem. C 118 (4) (2014) 1836–1842.
- [59] S. Atalay, Y.u. Ma, S. Qian, Analytical model for charge properties of silica particles, J. Colloid Interface Sci. 425 (2014) 128–130.
- [60] L.-H. Yeh, S. Xue, S.W. Joo, S. Qian, J.-P. Hsu, Field effect control of surface charge property and electroosmotic flow in nanofluidics, J. Phys. Chem. C 116 (6) (2012) 4209–4216.
- [61] G. Trefalt, S.H. Behrens, M. Borkovec, Charge regulation in the electrical double layer: Ion adsorption and surface interactions, Langmuir 32 (2) (2015) 380– 400

- [62] M. Nakamura, N. Sato, N. Hoshi, O. Sakata, Outer Helmholtz plane of the electrical double layer formed at the solid electrode-liquid interface, ChemPhysChem. 12 (8) (2011) 1430–1434.
- [63] A. Priye, W.H. Marlow, Computations of Lifshitz-van der Waals interaction energies between irregular particles and surfaces at all separations for resuspension modelling, J. Phys. D: Appl. Phys. 46 (2013) 425306.
- [64] V.B. Svetovoy, G. Palasantzas, Influence of surface roughness on dispersion forces, Adv. Colloid Interface Sci. 216 (2015) 1–19.
- [65] N. Eom, D.F. Parsons, V.S.J. Craig, Roughness in surface force measurements: Extension of DLVO theory to describe the forces between hafnia surface, J. Phys. Chem. B 121 (2017) 6442–6453.
- [66] F.L. Leite, C.C. Bueno, A.L. Da Róz, E.C. Ziemath, O.N. Oliveira, Theoretical models for surface forces and adhesion and their measurement using atomic force microscopy, Int. J. Mol. Sci. 13 (12) (2012) 12773–12856.
- [67] J.A. Alves Júnior, J. Baptista Baldo, The Behavior of zeta potential of silica suspensions, New Journal of Glass and Ceramics 4 (2) (2014) 29–37.
- [68] L. Liu, Z. Guo, Z. Huang, J. Zhuang, W. Yang, Size-selective separation of DNA fragments by using lysine-functionalized silica particles, Sci. Rep. 6 (2016) 22029
- [69] M.A. Brown, Z. Abbas, A. Kleibert, R.G. Green, A. Goel, S. May, T.M. Squires, Determination of surface potential and electrical double-layer structure at the aqueous electrolyte-nanoparticle interface, Phys. Rev. X 6 (1) (2016) 011007.
- [70] A.H. Jalil, U. Pyell, Quantification of zeta-potential and electrokinetic surface charge density for colloidal silica nanoparticles dependent on type and concentration of the counterion: Probing the outer Helmholtz plane, J. Phys. Chem. C 122 (8) (2018) 4437–4453.